Chapter 6
Interface Stability of Polymer and Small-Molecule Organic Photovoltaics

Degradation Mechanisms, Characterization Techniques, and Improvement Approaches

D. W. Zhao, L. Ke, W. Huang and X. W. Sun

Abstract In this chapter, the interface degradation mechanisms in organic photovoltaics (OPVs) will be discussed. The interface instability is mainly ascribed to the diffusion of oxygen and water into the electrode materials as well as the interface modification layer between electrode and organic layer. Furthermore, the commonly used characterization techniques are presented, which are quite helpful to understand the origin of the interface instability and their level of impact. In particular, these techniques reveal optical and electrical changes at the interface.

D. W. Zhao
School of Electrical and Electronic Engineering, Nanyang Technological University, Singapore 639798, Singapore
e-mail: dewei_zhao@hotmail.com

D. W. Zhao
Department of Electrical Engineering and Computer Science, The University of Michigan, Ann Arbor, Michigan 48109, USA

L. Ke
Institute of Materials Research and Engineering 3 Research Link, Singapore 117602, Singapore
e-mail: karen-kl@imre.a-star.edu.sg

W. Huang
Key Laboratory for Organic Electronics and Information Displays (KLOEID), Institute of Advanced Materials (IAM), Nanjing University of Posts and Telecommunications, 9 Wenyuan Road, Nanjing, Jiangsu 210046, China
e-mail: iamwhuang@njupt.edu.cn; wei-huang@njupt.edu.cn

X. W. Sun (✉)
Department of Electronic and Computer Engineering, South University of Science and Technology of China, Shenzhen, 518055 Guangdong, China
e-mail: xwsun@sustc.edu.cn

X. W. Sun
School of Electrical and Electronic Engineering, Nanyang Technological University, Singapore 639798, Singapore

W. C. H. Choy (ed.), *Organic Solar Cells*, Green Energy and Technology,
DOI: 10.1007/978-1-4471-4823-4_6,

Therefore, the analysis on the interface degradation and development of characterization techniques would contribute to the understanding of interface stability and further enhance the entire device lifetime.

6.1 Introduction

Polymer and small-molecule organic photovoltaics (OPVs) have been attracting great attention in the past few years due to their unique properties of low cost, easy process at low temperature, and flexibility. They are becoming one of the future photovoltaic (PV) technologies for the lowest cost clean energy production. The rapid increase of OPV efficiency from 1 % in 1999 to 8.33 % in 2010 has made the commercial products realistic [1–6].

The light harvesting of organic semiconductors can be tuned to match solar irradiative spectrum by chemical design and synthesis. The capability of being solution processed is the most potential for manufacture by printing or coating techniques, which significantly enhances possibility of realizing large-area and low-cost cells. To enter commercial PV market, OPVs have to satisfy a few basic and standard requirements in cost, efficiency, and lifetime. Actually, the low efficiency and short lifetime of OPVs are compensated by their low module cost, which provides a strong impetus to invest in OPV technology [7]. The low efficiency could be solved by organic semiconductor materials, transparent electrode, light management, device physics to drive the OPV technology toward much more developed.

One of the limitations to commercialization is the short lifetime or instability of OPVs. Typically, investigations on stability of OPVs have been focused on the effect of the water and oxygen on the degradation of photoactive layers and electrodes in encapsulated or unencapsulated devices under different environment conditions such as continuous illumination, oxygen, nitrogen, moisture, and vacuum [8], i.e., factors that affect stability are primarily oxygen, humidity, temperature, cycling of temperature, light, loading conditions, pre-treatment, packaging, electrodes, and so on. Figure 6.1 displays the effect of three main factors influencing device stability [9]. In general, most studies on degradation of OPVs are correlated with oxidative damage to the photoactive layer associated with illumination of the device in presence of molecular oxygen, and several light dependent degradation pathways have been identified [10–16]. It is well known that OPVs have to suffer a relatively high temperature during operation, which could also degrade organic photoactive materials and electrodes to a great degree. Since organic semiconductors are highly sensitive to photo-oxidation or photobleaching, encapsulation of OPVs is necessary, preventing the exposure of active materials and electrodes to oxygen and water. Additionally, polymerization-induced impurities have to be extracted as they are likely to form free radicals upon photolysis [8, 17].

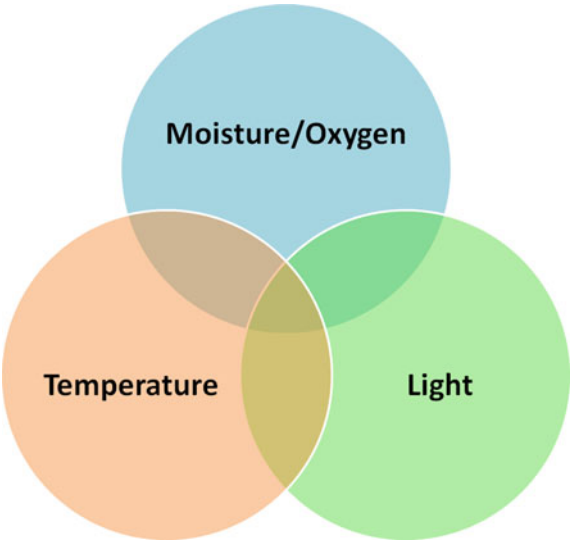

Fig. 6.1 The effect of three main factors that influence the device stability. The properties have been demonstrated separately, but usually they have a combined effect on the total device lifetime [9]

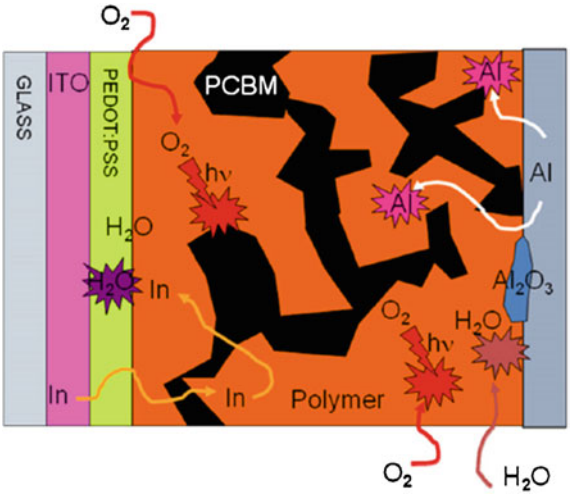

Fig. 6.2 A schematic illustration (cross-section view) of some degradation processes that take place in a typical bulk heterojunction (BHJ) OPV [8]. (Reprinted from [8], with permission from Elsevier) (http://www.sciencedirect.com/science/journal/09270248)

Figure 6.2 shows a cross-section view of the main processes that are considered to degrade OPVs. These processes represent extrinsic (diffusion of water and oxygen, mechanical stress, operation temperature under light illumination) and intrinsic mechanisms (photochemical degradation caused by singlet oxygen due to energy transfer from photoexcited polymer to adsorbed ground state oxygen molecules, movement of mobile species, such as indium and electrode materials like Al, interface degradation due to high energy excited stated chemistry at the interfaces and easy oxidization of metals, charge carrier density, and the morphology change of blend active layer) [8].

It is possible to classify the likelihoods of each mechanism as HIGH, MEDIUM, and LOW [9]. Diffusion of oxygen and water as well as electrodes (Indium Tin Oxide (ITO) and metals) possesses "HIGH" likelihood compared to other degradation mechanisms. It is obvious that the "HIGH" degradation has close relation with various interfaces. The "MEDIUM" likelihood of photo-oxidation of organic semiconductors and interfacial layer are followed. Furthermore, mechanical degradation has the relatively "LOW" likelihood. Therefore, the approaches to improve device stability can be conducted on the basis of likelihoods to overcome the degradation from the most significant level (HIGH) and to the least significant level (LOW).

Specifically, the efficient approaches to prevent the diffusion of oxygen and water are to develop mature device encapsulation to control the ability of O_2 oxygen transmission rate (OTR) and water water vapor transmission rate (WVTR) to cross an encapsulating membrane within a certain value, i.e., it is generally accepted that the lifetime of OPVs above 10, 100 h requires the upper limits of OTR of 10^{-3} $cm^3 \cdot m^{-2} \cdot day^{-1} \cdot atm^{-1}$ and WVTR of $10^{-6}g \cdot m^{-2} \cdot day^{-1}$, which are six to eight orders lower than the corresponding values of commercially available polymer films [18, 19]. The adhesives between layers should also be enhanced. Moreover, for electrode degradation, an alternative to ITO is remarkably required and interfacial engineering (hole-transporting layer (HTL)) is necessary correspondingly. On the other side, optimization of metal electrode such as electron-transporting layer (ETL) is of great importance to remain a good contact and insensitive to environment.

So far, there are many reports and reviews on study of device degradations [8, 20–23]. However, few reviews are concentrated on the effect of interface degradation on the device stability. In this chapter, we will mainly discuss the interface degradation mechanisms, followed by possible characterization techniques for detecting the change of interface structure. The understanding of interface degradation should serve as potential routes for improving interface stability and also entire device stability; therefore, highly promising improvement approaches of interface stability will be summarized. Finally, one of the challenging efforts on technology development is device encapsulation with low-cost and high-quality barrier. Thus, the encapsulation techniques will be introduced.

6.2 Mechanisms for Interface Degradation

For small-molecule organic light-emitting diodes (OLEDs), the luminescence degradation mechanisms have been systematically and comprehensively reviewed [20], which are mainly attributed to three individual and distinct modes as (i) dark-spot degradation, (ii) catastrophic failure, and (iii) intrinsic degradation. "Dark spots" refers to the formation of visible nonemissive defects or regions, leading to a decrease in device luminance due to the losses of emissive area. The underlying mechanisms might be electrochemical in nature or be thermally activated.

Catastrophic failure is primarily associated with defects existing in the organic active layers, resulting in a sudden decrease or total loss in luminescence as a result of large leakage currents due to electrical shorts. The underlying mechanisms are ascribed to morphological defects existing in organic layers or electrodes, or thermally induced during device operation with a temperature beyond glass transition temperature (T_g) of organic materials. The former two are considered to be correlated with surroundings. The intrinsic degradation, however, primarily material dependent, exhibit a progressive decrease in the brightness of the emissive area of a device with time during operation and no visible changes in device appearance. Aziz et al. attributed the intrinsic degradation to (1) the indium migration model, (2) the unstable cationic Alq_3 model, (3) the morphological instability model, (4) the immobile positive charge accumulation model, and (5) the mobile ionic impurities model.

For small molecules and polymer OPVs, they have similar device structures with OLEDs and also suffer similar issues associated with essential materials, electrodes, layer interface, and environmental conditions. In this section, we will focus on the discussion about the degradation mechanisms originating from interface instability at the adjacent layers such as anode and anode buffer layer, cathode and cathode buffer layer.

6.2.1 Anode and Anode Buffer Layer

ITO is the most commonly used anode for organic optoelectronic devices, which plays a significant role in injecting or extracting the holes from the active layer. Although ITO is relatively stable, it still suffers the degradation when exposed to special environments.

Carter et al. observed that the presence of ITO accelerates a long-term device failure in polymer OLEDs, induced by photo-oxidation of the light-emitting polymer via oxygen out of the ITO when polymer was fabricated directly onto ITO surface [24, 25]. The chemical reaction of the vinyl carbon with oxygen from the ITO anode induces the chain scission of active polymer [24]. Moreover, Stott et al. reported two major modes of degradations in ITO/MEH-PPV/Ca when they were operated in a dry inert atmosphere [24]: one originating from the oxidization of polymer MEH-PPV is likely caused by diffusion of the oxygen from ITO, resulting in luminescence quenching and increased impedance due to formation of aromatic aldehyde and chain scission, respectively; the other one is attributed to localized microscopic electrical shorts, however these shorts do not cause immediate failure of devices since self-induced fusing of the surrounding cathode metal isolates the shorts, which decreases the effective active area of each device. Only when the region of damaged cathode starts to coalesce does the ultimate failure happen.

Moreover, Krebs et al. found ITO etching indirectly due to the indium diffusion into the layers of device Al/C_{60}/P3CT/ITO [26]. The observation is the fact that

indium diffuses through all layers in the device and ends up on the outer surface of the counter electrode (Al).

It is clear that the interface between ITO and active layer is playing an important role in device performance and lifetime. Therefore, one effective solution is to incorporate poly(3,4-ethylenedioxythiophene):poly(styrenesulfonate) (PEDOT:PSS) as anode buffer layer between ITO and photoactive layer, which results in obvious improvement of lifetime and luminous efficiency [25]. Choice of polyaniline doped with conducting PSS could partially overcome the issue associated with the ITO/organic interface instability. Consequently, PEDOT:PSS has been widely used in organic electronic devices with the functions of (1) a barrier to prevent oxygen reaction, (2) a planarizing layer to inhibit electrical short points, (3) an interfacial layer to shift the work function of ITO, and (4) an adhesive layer to facilitate the adhesion between ITO and active layer [27]. The incorporation of PEDOT:PSS layer could also prevent the diffusion of indium containing etch products into organic active layer by trapping them.

However, the interface instability caused by PEDOT:PSS exists as well. de Jong et al. studied the interface stability between ITO and PEDOT:PSS by using Rutherford backscattering (RBS) [28]. It is found that the indium concentration in PEDOT:PSS increases from 0.02 to 0.2 at.% upon annealing in nitrogen at 100 °C for 2500 h. A more serious and faster degradation of ITO/PEDOT:PSS interface is observed when exposed to air, and the indium concentration reaches a saturated value of 1.2 at.% after a few days. Therefore, it is explained that the strong acidic nature of PEDOT:PSS makes the ITO etched. Furthermore, Girtan et al. compared two sets of devices with ITO/PEDOT:PSS or only PEDOT:PSS as transparent anode using MDMO-PPV:C_{60}BM or P3HT:PC_{60}BM blend system as the active layer [29]. It was found that V_{oc} of cells without ITO stays unchanged after aging (40 days in open atmosphere at room temperature) and this is not valid for cells with ITO. Meanwhile, for cells without ITO, the J_{sc} decreases by one or two orders of magnitude after aging, by contrast, for cells with ITO, the J_{sc} decreases by four to seven orders of magnitude. The results show that the work function of ITO changes with surface modification during aging. Kawano et al. studied the degradation of nonencapsulated OPVs (ITO/PEDOT:PSS/MDMO-PPV:PCBM/Al) under different ambient conditions such as white light irradiation, in dark, exposure to air, dry oxygen, and humid nitrogen atmospheres [30]. By comparing the devices with and without PEDOT:PSS, the main reason for degradation under air exposure is ascribed to water adsorption by the hygroscopic PEDOT:PSS layer, independent of light, therefore, the resistance at the PEDOT:PSS/blend layer interface is increased with degrading, proved by the change of charge mobility and hole injection after air exposure. Spatially inhomogeneous degraded PEDOT:PSS layer is correlated with insulating domains causing current loss.

Thus, it is summarized that the interface degradation caused by PEDOT:PSS should be as follows: (1) the ITO etching due to acidic nature of PEDOT:PSS; (2) the resistance increase due to the water adsorption by hygroscopic PEDOT:PSS; (3) the change of ITO work function due to aging.

6.2.2 Cathode and Cathode Buffer Layer

Low work function (LWF) metals, such as Ca, Mg, and Al, are used to inject or collect electrons as cathode. It is known that LWF metals are prone to be oxidized and to cause device degradation due to the diffusion of oxygen and water into itself or organic active layer. Moreover, at the organic/metal interface, instability might exist due to the intrinsic or extrinsic properties of metals. In order to achieve matched energy levels of organic layer and metal, a few interfacial layers can be incorporated in between organic active layer and metal to improve the charge injection or collection.

Aziz et al. studied the main mechanisms of degradation in OLEDs (ITO/PPV/Al), concluding that the electrochemical reaction between two electrodes is found to be a major cause, resulting in corrosion and microstructural changes in both electrode materials [20, 31, 32]. Therefore, the electrode materials can degrade significantly forming a complex with electrolyte-like polymer, leading to the increase of threshold voltage. At the same time, the additional conditions such as moisture or impurities in polymers will enhance the ionic conductivity of the active layer and accelerate the corrosion of the electrode at the affected locations. Subsequently, Aziz et al. further investigated the degradation mechanism in Alq_3 based OLEDs [32]. The results indicate that the short lifetime is mainly caused by the injection of holes into Alq_3, leading to a decrease in fluorescence quantum efficiency due to unstable cationic Alq_3 species as well as fluorescence quenching sites. Therefore, many stabilized OLEDs by doping the hole-transporting layer, or using a buffered hole-injection contact, or forming alternating hole and electron transporting based emitting layers, can be explained reasonably and correspondingly.

For OPVs, as investigated by Reese et al., the conclusion has been drawn that the organic/metal interface is a major source of device degradation for P3HT:PCBM OPVs [33, 34].

Krebs et al. systematically investigated the stability of MEH-PPV:PCBM-based devices in terms of atmosphere, handling, electrode treatment, mode of preparation, and barrier layers by the dependence of J_{sc} on time [15]. The authors separate various degradation processes responsible for the decay and carry on the study with the model of $I_{sc}(t)/I_{sc}(0) = Ae^{-bt} + Ce^{-dt} + \cdots$, where b and d are the time constants, A and C are the weighting of the individual exponential functions [15]. It is expected that individual responsibility for the device degradation could be linked to the experimental parameters by making changes correspondingly. These experimental parameters can be selected separately and in parallel. Then, the integrated charge could be achieved by $Q_{total} = A/b + C/d + \cdots$ when extrapolated to infinity [15]. Similarly, the degradation of P3HT:PCBM-based OPVs can be represented by an exponential term describing the fast initial decay and a second exponential term describing the long-term degradation, as $\eta = \eta_0[ae^{-\gamma t} + be^{-\delta t}]$, where η_0 is the initial efficiency and a, b, γ, δ are curve fitting parameters [35, 36]. The time constant γ indicates the fast decay process of degradation and γ is related to a slow decay. Schuller et al. developed various models for dynamic degradation, including

both a single exponential mode and a linear mode in which the latter one is preferred [37]. However, Krebs et al. found that such a linear model could represent degradation well only at the beginning of the device life [15], therefore it is suggested that a single exponential could be a good fitting in a few examples and several exponentials could fit better. It is found that the decay curves could be fitted with a two-term exponential function: an initial fast decay and a second slower decay. The fast decay is independent on atmospheric conditions such as device operation and various barrier layers at the active layer/Al interface. The slow decay depends on the atmosphere due to the reaction with oxygen [15].

Logdlund et al. demonstrated a theoretical investigation on the interaction of Al with PPV and its derivatives [38]. It is found that Al prefers the reaction with vinylene linkages in methoxy groups based PPV materials via forming covalent bonds, Al–C. This is actually useful for cathode in OPVs due to the LWF of Al. However, when methoxy groups are replaced with carbonyl groups, new reactive sites are induced, resulting in Al–O bonds and exhibiting comparable stability. Moreover, another explanation is proposed to be the existence of electron charge transfer from the Al atoms to the polymer chains. Karst et al. studied the small-molecule OPVs (ITO/PEDOT:PSS/CuPc/PTCDA(or DAAQ)/Al) with upper Al electrode exposed to air [39]. The results show that the device with no exposure to air yields a small V_{oc} (0.125 V), and meanwhile, the V_{oc} (0.5 V) increases largely when the device is exposed to air as a result of an oxide layer (probably Al_2O_3) present at the Al/organic interface. It is explained that the direct contact of organic acceptor with Al or Ag induces Fermi level pinning, resulting in small V_{oc}. Formation of such an oxide layer separates the organic and Al layers, leading to no more Fermi level pinning and high V_{oc}.

Jeranko et al. demonstrated decay processes by using two-dimensional mapping of PV response on the active area, concluding that a major degradation is attributed to the path along the edges of the active area and the variance in the photocurrent over the area of the device caused by the process of electrodes [12, 15].

A cathode buffer layer is essentially necessary for good charge extraction by cathode. Usually, it is thin enough to possibly prevent the opposite charge from being injected or collected due to the existence of energy barrier at the organic/metal interface.

Melzer et al. discussed the effect of inserting a C_{60} layer in between active layer and cathode by *I–V* characteristics and impedance spectroscopy, suggesting the presence of a strong dipole layer at the C_{60}/metal interface [40]. Krebs et al. also inserted a C_{60} layer at the MEH-PPV/Al interface [15], therefore, a significant improvement on device stability is observed on the first decay parameter due to the formation of an efficient barrier layer that conducts the electrons well and facilitates the exciton dissociation. Moreover, the authors claimed that high current density due to high illumination intensity could accelerate the degradation, indicating that the weight of the first exponential increases with the illumination intensity. This could be attributed to chemical reactions of photoinduced radical anions and radical cations at the Al interface. The concentration of charge carriers at the Al surface increases with the current density increasing, resulting in the

saturation of surface density and possible increase in chemical degradation. In addition, the effect of temperature on device degradation was studied by setting up a temperature-controlled platform via a fan for the measurement of the devices. It is confirmed that a higher temperature accelerates device degradation, which is correlated with glass transition temperature (T_g) of the polymer. It means if a fast degradation of devices at an operation temperature close to T_g could be observed, the motion of polymer chains is increased and the electrode diffuses.

BCP is also an effective electron-transporting material as an exciton-blocking layer and electron-transporting layer in organic optoelectronic devices. Vogel et al. [41] incorporated BCP buffer layer at the C_{60}/Al interface in small-molecule OPVs (ITO/PEDOT:PSS/Pc/C_{60}/BCP/Al) to reduce exciton quenching at the C_{60}/Al interface and to enhance electron transport from C_{60} to Al due to established Ohmic contact between C_{60} and Al, resulting in a significant improvement of efficiency. However, BCP does not have effect on blend geometry based OPVs (ITO/PEDOT:PSS/Pc:C_{60}/BCP/Al). Moreover, BCP prevents the diffusion of Al during deposition on top of C_{60} film, creating a highly structured interface. BCP also blocks the exciton recombination caused by chemical reactions which forms recombination centers at the interface.

An alternative to current organic electron-transporting materials is an insulator, such as Al_2O_3 or LiF, as cathode buffer layer. Zhang et al. found Al_2O_3 in a role of improving electron injection at the organic/cathode interface in Alq_3 based OLEDs [42]. The fact that holes are injected and accumulated at the organic/buffer interface could be beneficial to the enhancement of electron injection due to the tunneling barrier reduction by changing the Fermi level of the cathode and carrier transporting models. Hung et al. [43] demonstrated that an ultrathin LiF layer at the organic/Al interface enhances electron injection and electroluminescence efficiency in an OLED of ITO/CuPc/NPB/Alq_3/LiF/Al, which is primarily attributed to band bending of the organic active layer by more than 1 eV when Alq_3 contacts with the dielectric LiF, resulting in the reduction of electron injection barrier height at Alq_3/Al interfaces.

Brabec et al. summarized a few mechanisms of LiF used in organic electronic devices [44]: (1) lower the effective work function of Al; (2) dissociated LiF reacts with the organic layer via chemical doping; (3) form a dipole layer to make a vacuum level offset between organic layer and Al; (4) protect the Al atoms from diffusing to organic layer during thermal deposition. Subsequently, Brabec et al. [44] inserted an ultrathin LiF layer between BHJ active layer and metal cathode (Al and Au) to largely enhance the FF and to stabilize high V_{oc}. They proposed a combined mechanism of the formation of a dipole moment across the junction, due to either orientation of the LiF or chemical reactions leading to charge transfer across the interface. An alignment of LiF is ascribed to the fact that the Li^+ adheres preferably to the organic surface and the F^- points toward the Al surface. Furthermore, van Gennip et al. [45] studied and confirmed the mechanism of LiF at the interface of metal and active layer by using secondary ion mass spectrometry (SIMS) and X-ray photoelectron spectroscopy (XPS) measurements. SIMS spectra measured at the organic/LiF interface to determine the chemical state of LiF layer

on the surfaces of MDMO:PPV and PCBM substrates, showing that AlF_3 is absent at the Al/LiF/MDMO-PPV and Al/LiF/PCBM interfaces, proving that the occurrence of the reaction is missing, which is used to explain the improved electron injection and collection. Moreover, a reaction of Al with carboxylic oxygen of PCBM actually takes place, proved by XPS measurements; however, this reaction is inhibited by LiF layer at the PCBM/Al interface.

6.3 Characterization Techniques for Interface Degradation

Highly efficient characterization techniques for interface degradation are very significant in order to understand the variance of interfaces during the device operation and their correlation with device degradation [8].

In OLEDs, Aziz et al. [31] employed characterization techniques, such as impedance spectroscopy (IS), electrochemical measurement, and scanning electron microscopy (SEM) to provide a mechanistic picture for degradation process. Experimental observations are analyzed and correlated to reveal the presence of an electrochemical reaction which causes device failure.

Jorgensen et al. summarized the characterization techniques and classified them into two typical ones [8]: one is including the approaches which could offer morphological and chemical information from specific locations in the device; the other one is covering the approaches which provide information from nonspecific locations in the device, i.e., information from all layers or the whole averaged analysis over a large area. The characterization techniques from the specific locations are typically time-of-flight secondary ion mass spectrometry (TOF-SIMS), depth profiling, XPS, atomic force microscopy (AFM), SEM, interference microscopy, fluorescence microscopy, and RBS. Meanwhile, the characterization techniques from the nonspecific locations are usually IS, near-field scanning microscopy (NSOM), infrared spectroscopy (IRAS), X-ray reflectometry (XRR). In addition, various ambient conditions such as white light irradiation, in dark, exposures to air, dry oxygen, and humid nitrogen atmospheres, can be applied to support the characterization of device degradation [30].

In this section, we will emphasize the characterization techniques for interface degradation and their corresponding analysis divided into optical and electrical aspects.

6.3.1 Optical Techniques

It is easily understood that optical techniques are based on the optical characterization and measurement of degradation and provide information about the correlation between interface variance and device degradation.

NSOM is used to establish the relation between morphology of BHJ and photocurrent generation. It is a potential technique to characterize the solar cells at the nanoscale level although it does not conclude the influence of device morphology on the device degradation and only shows the possibility [8, 46].

X-ray reflectometry or X-ray reflectivity (XRR) technique is used to probe the interfacial properties of layered samples such as films on substrates, multiple layers, and superlattices, which is based on Snell rule [47]. In the energy dispersive (ED) mode, a polychromatic primary X-ray beam is used and the reflection patterns are collected at a fixed angle, by an ED solid-state detector [48, 49]. The in situ EDXRR could overcome the issues associated with probable intrinsic errors in removing and repositioning the samples and allow the high-accuracy recording of the film morphology with the time evolution [50]. It is said that the in situ EDXRR technique is a powerful nondestructive tool to study the aging effect at the interface of OPVs under working conditions.

Paci et al. studied the evolution of the morphology in OPVs of glass/ITO/MDMO-PPV:PCBM/Al during operation by using EDXRR, in which three steps are included [50]. The first step is a preliminary set of XRR measurements on three different samples ((1) Glass/ITO/MDMO-PPV:PCBM; (2) Glass/ITO; (3) Glass/ITO/MDMO-PPV:PCBM/Al), representing the successive stages of cell construction, which identifies the contributions from each layer to the overall cell reflection patterns and provides accurate data regarding the electronic densities of the different layers. The second step as shown in the inset of Fig. 6.3 is the verification of morphological stability of the device under ambient condition, representing repeatable measurements even after a few months. The third step shown in Fig. 6.3 is a collection of XRR results and patterns on an OPV, measured under controlled atmospheric conditions, i.e., both in the dark and during 15 h illumination, leading to systematically morphological variation at the electrode/organic layer interface. Therefore, it is concluded that the direct correlation between progressive thickening of this interface and the decrease in device performance, explained by a "real" effect—the formation of an Al oxide layer at the film surface and at the interface with organic active layer due to a photo-oxidation reaction, or a possible but indistinguishable change of the formation of a layer at the Al/organic interface due to indium diffusion from the ITO.

Paci et al. further confirmed the photoinduced oxidation of the metal electrode at the organic/metal interface by using EDXRR technique in cells without (Cell A) and with (Cell B) protection layer of LiF at the organic/metal interface [51]. It was suggested that the Al oxidation in Cell A is correlated with the first aging process exhibited by the exponential decay in Fig. 6.4. Meanwhile, Cell B does not show the same two-step process, exhibiting no loss of efficiency in the first 15 h due to the stable morphology at the LiF/Al interface and also the absence of oxidation process. Therefore, the insertion of LiF is beneficial to the protection of the fast photoinduced degradation in the first few hours. As highlighted by the authors, the conclusion that the formation of oxidization layer between organic layer and metal is prevented by inserting a LiF buffer layer has been drawn under the real-time in

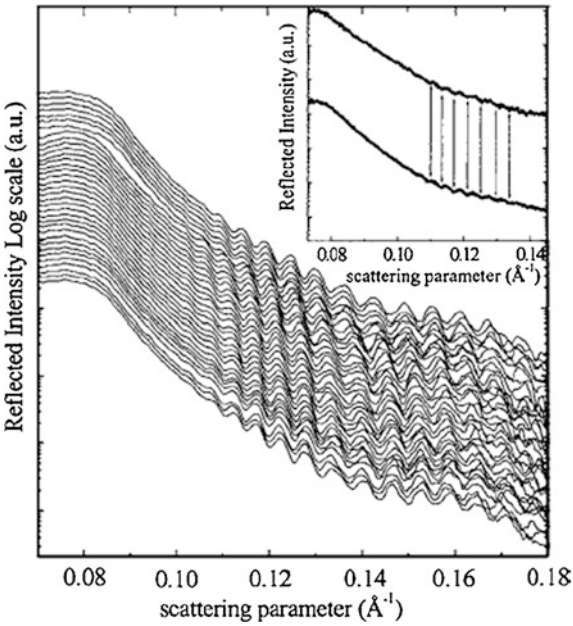

Fig. 6.3 In situ EDXRR measurements of the solar cells, collected under controlled atmosphere and upon illumination. The reflectivity profiles are shifted in height for clarity. Inset: the ex situ EDXRR measurements carried out at a distance of several months on the same cell [50]. (Reprinted with permission from Ref. [50]. Copyright [2005], American Institute of Physics)

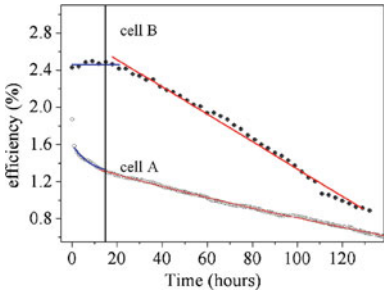

Fig. 6.4 Efficiency curves for cell A and cell B [51]. (Reprinted with permission from Ref. [51]. Copyright [2006], American Institute of Physics)

situ EDXRR measurements without any complementary technique for additional study on morphology and structure.

However, there is a contradictory discussion that Andreasen et al. [52] cannot correlate the fast degradation of OPVs to a substantial change of morphology, verified by XRR technique, instead the authors found that rough interfaces of stacking layers significantly inhibits the resolution of the XRR technique for in situ investigation on physical degradation mechanisms, implying that it is difficult to detect the changes at the interface of multiple layer-based OPVs (ITO/PEDOT:PSS/MEH-PPV:PCBM or P3HT:PCBM/Al) although different model fittings have been applied.

XPS is a quantitative spectroscopic technique measuring the elemental composition, empirical formula, chemical state, and electronic state of the elements in a material, which is performed under ultra-high vacuum. XPS is used to analyze

the surface chemistry with a probe depth of 1–10 nm away from the top. It is also used to analyze the elements giving information on the chemical state [8]. Gennip et al. [45] used XPS to detect and confirm the reaction of Al with the carboxylic group (O 1 s carboxylic oxygen peak) present in PCBM so that a LiF layer at the PCBM/Al interface blocks this reaction.

SIMS is the most sensitive surface analysis technique to analyze the composition of solid surfaces and thin films by sputtering surface of the specimen with a focused primary ion beam and collecting and analyzing ejected secondary ions. The measured secondary ions with a mass spectrometer are used to determine the elemental, isotopic, or molecular composition of the surface. TOF-SIMS is a method of mass spectrometry in which an ion's mass-to-charge ratio is determined via a time measurement. More importantly, TOF-SIMS technique is superior to XPS in view of the imaging capabilities and the sensitivity [8]. Gennip et al. [45] measured SIMS to show that LiF does not react with aluminum to form AlF_3, nor does it react in any other way to liberate Li, as mentioned in Sect. 2.2. Much more details on optical techniques for degradation characterization can be found in ref [8].

6.3.2 Electrical Techniques

Electrical techniques are based on the information provided by the characterization and measurements of electrical properties, which can be able to reveal the change of interface state and their influence on the interface stability.

Impedance spectroscopy (IS), also known as electrochemical impedance spectroscopy, measures the dielectric properties of a medium as a function of frequency. It is based on the interaction of an external field with the electric dipole moment of the sample. It is also widely applied in a broad field of inorganic, organic, and biological systems based devices.

In BHJ OPVs, IS is commonly used to study the electrical transport properties [8]. An equivalent circuit, as shown in Fig. 6.5, is modeled to translate the frequency response of the circuit to the correspondingly individual interfaces and consequent layers in the devices. In this case, the dielectric constants for various materials could be found via changing the film thickness and fitting the experimental data [53], such as the distributed resistors r_t (representing the electron transport), the distributed chemical capacitance $c_n = C_\mu$ and r_{rec} (representing the electron recombination resistance), a series resistance R_s (representing the contact and wire effects), a capacitor $C_g \approx \varepsilon\varepsilon_0 A/L$ (representing dielectric contribution of the diode), and two corresponding characteristic times: electron diffusion $\Gamma_g = r_t c_n$ (transit time) and effective lifetime $\Gamma_n = r_{\text{rec}} c_n$, respectively [53, 54]. In typical OPVs, due to special conditions during deposition of Al layer, the nature of the Al/polymer interface plays a key role in the electron and hole transfer. IS can also be used to monitor the effect of the annealing progress.

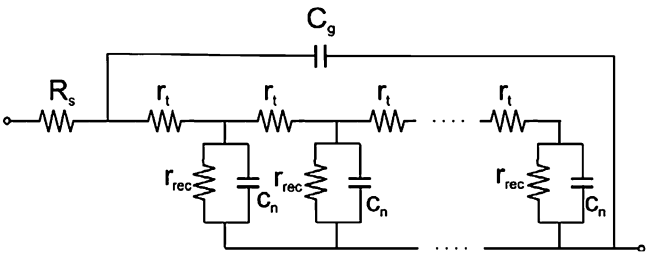

Fig. 6.5 An equivalent circuit accounting for the diffusion–recombination mechanism used for fitting. Modulation of stored excess minority carriers gives rise to distributed chemical capacitance c_n. Bimolecular recombination of conduction band electrons and valence band holes are modeled by resistive elements r_{rec}. Transport of electrons is represented by means of r_t. An additional series resistance is needed to model contact and wire effects, R_s. Finally, a capacitor $C_g \approx \varepsilon\varepsilon_0 A/L$ represents dielectric contribution of the diode [53]. (Reprinted from [53], with permission from Elsevier) (http://www.sciencedirect.com/science/journal/15661199)

There has been a very detailed review on application of IS technique in dye-sensitized solar cells (DSSCs), quantum dot based dye-sensitized solar cells (QD-DSSCs), and OPVs [55]. Fabregat-Santiago et al. speculated the understandings of measured capacitance as a function of voltage and IS spectra [55]. First, they summarized a characteristic measurement as shown in Fig. 6.6a and the subsequent four feature regions that can be distinguished as follows:

(I) at a large reverse bias ($V_{app} \ll V_{fb}$), the sample is considered as a dielectric capacitor with a constant capacitance, giving rise to a geometrical value C_g;
(II) at a moderate reverse and low forward bias ($V_{app} < V_{fb}$), the C–V characteristic is close to a Mott–Schottky model ($C_{sc} = A\varepsilon_r\varepsilon_0/W = A\varepsilon_r\varepsilon_0/W_0V_{sc}^{1/2}$), as shown in Fig. 6.6b, where C_{sc} is determined by the depletion layer modulation.
(III) at a proper forward voltage ($V_{app} \geq V_{fb}$), the capacitance (C_μ) is controlled by a chemical capacitance due to the excess carriers, which results in the collapsed depletion zone.
(IV) at a larger forward bias ($V_{app} \gg V_{fb}$), the capacitance goes saturated and finally decreases exhibiting negative limitation mechanisms.

Secondly, the authors present their interpretation on typical IS spectra, recorded under open-circuit conditions by varying the illumination level and characterized by a major RC arc plus additional minor features at high frequency [55, 56]. Generally, the information of charge transport, series resistance, and dielectric contributions might be reflected by the high-frequency arc of the spectra [53]; on the other hand, the recombination in the active layer will lead to the low-frequency arc of the spectra [57]. The values of the capacitance, resistance, and lifetime can be plotted as a function of V_{oc}.

Glatthaar et al. studied the effect of post-treatment on P3HT:PCBM BHJ OPVs by using IS [58]. The results indicate that a reduced doping level at the Al interface is observed as a depletion region evidenced by the bias dependence of IS (Fig. 6.7), leading to an improved rectification behavior at the organic/metal

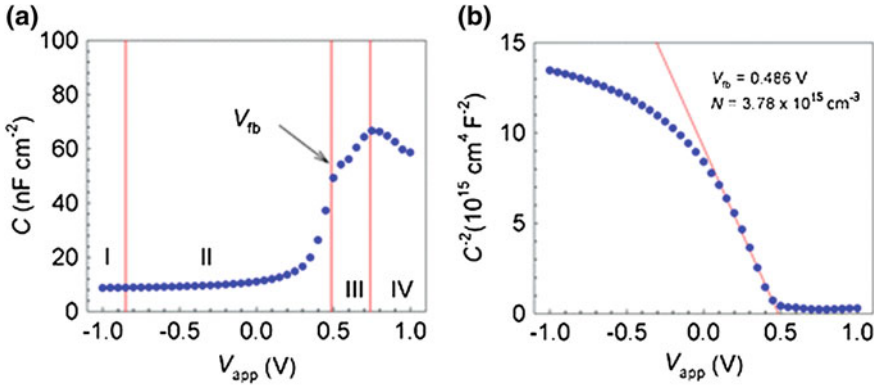

Fig. 6.6 **a** Characteristic capacitance response (100 Hz) of a device (ITO/PEDOT:PSS/P3HT:PCBM/Al), as a function of bias voltage. Vertical lines separate voltage regions for different capacitances. **b** Mott–Schottky curve (100 Hz) which exhibits a straight line from which the values $V_{fb} = 0.49$ V and $N_A = 3.8 \times 10^{15}$ cm^{-3} are determined, assuming $\varepsilon = 3$ for P3HT:PCBM [55]. (Reproduced by permission of the PCCP Owner Societies)

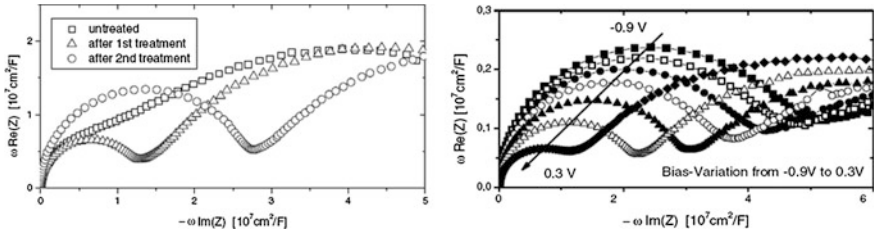

Fig. 6.7 (*left*) IS in the dark of the nontreated device, after the first post-treatment (30 s at 110 °C and 1 V forward bias) and after the second post-treatment (450 s at 110 °C and 2 V forward bias); (*right*) IS after the two consecutive post-treatment steps at different bias voltages [58]. (Copyright John Wiley and Sons. Reproduced with permission)

contacts. The device performance is also likely enhanced by the large space charge region and a positive doping gradient toward the hole contact due to the post-treatment, where charge separation is improved and electron recombination is reduced at the hole contact side due to possible electron transport in PEDOT:PSS layer.

Furthermore, Glatthaar et al. demonstrated that electrical IS can be a useful tool to identify two limiting factors in OPV efficiency by providing information about the conductivity of different regions within the device [59]. One is that the existence of *p*-type impurity doping in organic semiconductor results in a Schottky type contact at the Al interface, decreasing the charge collection efficiency and photocurrent, as there is no electrical field in the bulk region, which facilitates the charge separation. The other one is that a poor interface is permeating charge carriers due to the Al corrosion, leading to low FF. The authors explained that

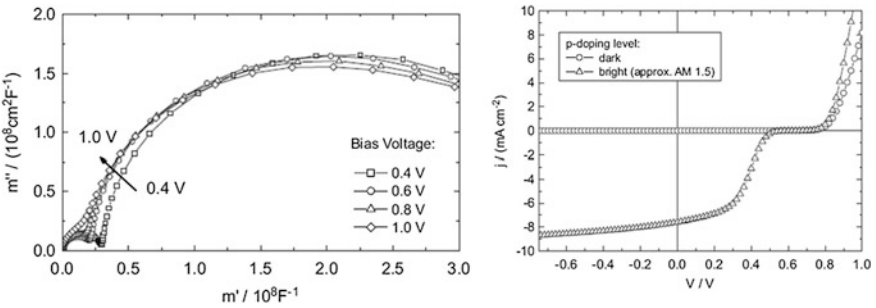

Fig. 6.8 (*left*) Electrical impedance of an inverted layer sequence device, where a TiO_2 layer was added between the electron contact of Ti and the absorber. In the modulus-plot, a semicircle can be observed at high bias, where built-in potential should be compensated and thus, the depletion region being vanished; (*right*) Modeled I–V curve of a device with a low extraction/injection rate for both charge carrier types at the electron contact [59]. (Reprinted from [59], with permission from Elsevier) (http://www.sciencedirect.com/science/journal/09270248)

the kink of *I–V* curve under illumination is caused by a slow charge transfer at the Al/organic interface, evidenced by the large capacitance for low frequencies as shown in Fig. 6.8 (left) due to the accumulated charges injected from the good contact at the blocking contact. Additionally, a one-dimensional model for such *I–V* curves, as shown in Fig. 6.8 (right) was developed by selecting small extraction velocities for the charge transfer at one interface (10^{-4} cm/s instead of 1000 cm/s). Both experiments and simulations are in good agreement.

6.4 Improvement Approaches to Interface Stability

6.4.1 Interface Engineering

In order to improve the interface stability, one effective way is to introduce a stable interfacial layer in between electrodes and organic photoactive layer. On the one hand, an air-stable *n*-type metal oxide can be inserted between active layer and Al cathode to replace the commonly used Ca or other LWF metals. On the other hand, at the anode side, an alternative to current PEDOT:PSS is *p*-type-like or transition metal oxides as the interfacial layer.

6.4.1.1 Cathode Buffer Layer

Wang et al. presented an extended lifetime of P3HT:PCBM-based BHJ OPVs by inserting a thin layer of CuO_x in between active layer and Al cathode, which was fabricated by thermal evaporation [60]. Figure 6.9 shows the comparison of various parameters as a function of storage time for the OPVs with the interfacial

layer of LiF, CuO_x, CuO_x/LiF, LiF/CuO_x. The device degradation is strongly dependent on the decrease of the photocurrent during the storage time. The results indicate that the CuO_x functions not only as a charge transport layer but also as a protection layer, preventing the formation of thick organic/Al interdiffusion area. Thus, an air-stable cathode/organic interface is achieved. Wang et al. also found chromium oxide (CrO_x) as Al cathode interfacial layer to improve the efficiency and stability in air since the device stability of OPVs depends on the cathode interfacial layers [61]. Devices with CrO_x exhibit higher PCEs and stability than those without CrO_x, showing improved stability 100 times better than those of devices without CrO_x or with LiF. It is likely attributed to the function of CrO_x as an electronic tunneling layer for electron collection and a protective layer for minimizing the damages caused by evaporating Al and also blocking diffusion of oxygen and water.

Insertion of an interfacial layer such as CrO_x and CuO_x is to effectively prevent diffusion of Al into the organic layer and thus to eliminate formation of the insulating layer that makes the device degrade. It is noted that diffusion of Cu atoms into the organic layer may also occur. However, the oxidation of Cu leads to

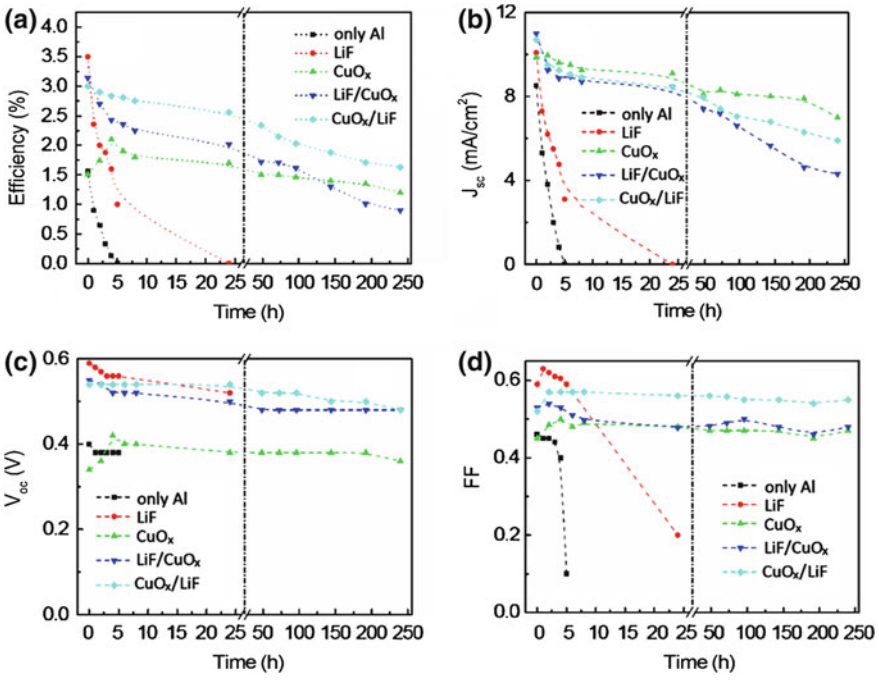

Fig. 6.9 Comparison of the **a** PCE, **b** (J_{sc}), **c** (V_{oc}), and **d** FF as a function of storage time for polymer solar cells without interfacial layer (only Al), with interfacial layer of LiF, CuO_x, CuO_x/LiF, LiF/CuO_x. Note that the device characteristics are monitored with increasing storage time for the same device [60]. (Reprinted with permission from Ref. [60]. Copyright [2011], American Institute of Physics)

a less insulating material as compared to Al_2O_3, likely explaining the slow degradation of the devices in air [60, 61].

Kim et al. produced a TiO_x layer by sol–gel procedure to modify the interface of P3HT:PCBM and Al cathode [62]. This TiO_x layer plays multiple functions as electron-transporting layer, hole- and exciton-blocking layer, optical spacer, and protecting layer during metal deposition. TiO_x layer serves to passivate the devices against intrusion of water vapor and oxygen, leading to remarkable enhancement of operation lifetimes [63, 64]. Moreover, the mechanism is proposed to be ascribed to oxygen deficiencies in the TiO_x film allowing adsorption sites for O_2 [62, 65]. Lee et al. investigated the correlation between TiO_x layer as optical spacer and the processing additive 1,8-octanedithiol [66]. The results indicate that the processing additive causes relatively rough surface of P3HT:PC_{60}BM film and reduces the effect as an optical spacer. Therefore, the dependence of processing additive on surface roughness also influences the interface stability.

Li et al. reported a study of the stability of OPV under air and UV irradiation, which consists of P3HT:PCBM as the active layer and 20 nm TiO_x as the protection layer prepared by partial hydrolysis of Ti-alkoxide in air [35], as shown in Fig. 6.10. It is stated that TiO_x as the protection layer could make significant improvement of device stability under air and UV exposure, implying a faster decay due to UV exposure compared to air.

Figure 6.11 shows the dependence of main parameters of OPVs on UV exposure time. It is clearly seen that the major loss in device efficiency under UV irradiation is induced by the decrease in the J_{sc} and the FF. Meanwhile, the V_{oc} remains essentially constant. Similar results happen to the air-exposure conditions. The measurements by transmission IR, UV spectroscopy, and ERS spectroscopy, indicate that the sol–gel derived TiO_x serves as an effective passivation film to prevent oxygen when exposed to light due to the photo-oxidation of the bound organic moieties causing oxygen gas scavenging [35]. The improvement mechanism behind by using TiO_x can be explained as [35]: the photochemical activity of a TiO_x film covers both Ti–OR functionalities and Ti–OH groups. From the results of IR spectroscopy, it is found that the residual Ti–OR functionalities bound into the sol–gel film are photo-oxidized, consuming O_2 (gas) and producing CO_2 (gas)

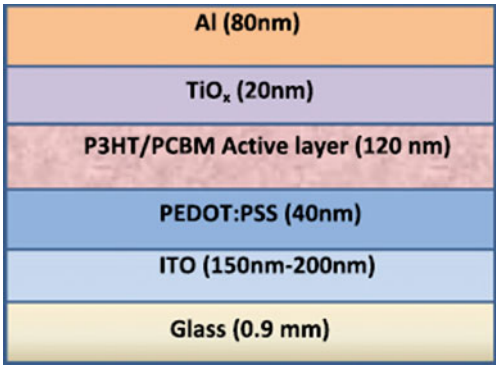

Fig. 6.10 OPV device structure [35]. (Reprinted from [35], with permission from Elsevier) (http://www.sciencedirect.com/science/journal/09270248)

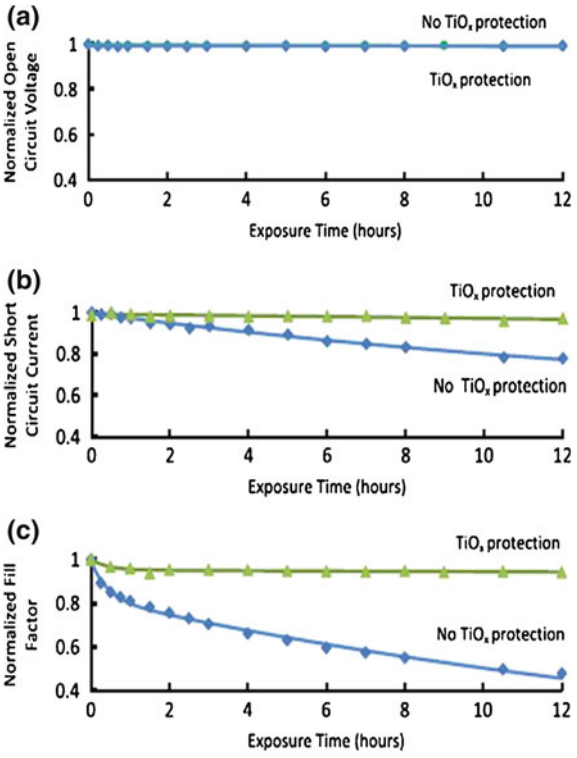

Fig. 6.11 Variance of **a** Voc, **b** Jsc, **c** FF with UV exposure time when sample was surrounded by nitrogen atmosphere (UV power density = 10 mW/cm2) [35]. (Reprinted from [35], with permission from Elsevier) (http://www.sciencedirect.com/science/journal/09270248)

and H_2O (gas), as well as bound format [HCOO–], H_2O, and Ti–OH moieties. The photoactivation of these films leads to O_2 scavenging and forms the basis for thin films, which removes oxygen upon exposed to light, thereby protecting an underlying surface from oxygen gas.

It is worth mentioning that the TiO_x film has a capacity of the order of 10^4–10^5 times the quantity of O_2 needed to seriously influence the organic active layer. Additionally, the TiO_x film will act as a diffusion barrier for oxygen, thus further slowing down the oxygen interaction with the active layer.

6.4.1.2 Anode Buffer Layer

Carter et al. shown polyaniline and polyethylenedioxythiophene based polymer transparent electrodes as hole-injecting anodes by replacing ITO in polymer OLEDs [25]. By varying the dopants of anodes, improved device performance was found independent of film conductivity, morphology, and type of conducting polymer. The results demonstrated that polymer anodes (1) create a clean repeatable surface without oxidation or water, facilitating the adhesion to polymer MEH–PPV; (2) partially dope the interface, forming Ohmic contacts and good

hole injection into electroluminescent polymer. These devices without ITO show a remarkably slower degradation.

Since PEDOT:PSS is a water-based solution with slight acidic nature, it is easy to cause interface instability associated with the etching of ITO and the diffusion to photoactive layer upon water adsorption. *p*-type like or transition metal oxides, such as MoO_3, V_2O_5, and WO_3, are becoming the most promising replacement of PEDOT:PSS as anode buffer layer to overcome the interface instability. Shrotriya et al. demonstrated transition metal oxides MoO_3 and V_2O_5 to replace PEDOT:PSS, forming Ohmic contact between active layer and ITO and improving device efficiency [67]. Recently, many investigations have involved transition metal oxides to enhance the hole transport/collection and extend the lifetime of device operation [68–71].

Sun et al. combined both benefits of anode and cathode interfacial layers MoO_x and TiO_x to obtain efficient and air-stable BHJ OPVs based on PCDTBT:PC_{70}BM [72], as shown in Fig. 6.12 (left). Figure 6.12 (right) shows the comparison of the air stability of PCDTBT:PC_{70}BM devices fabricated with a 9 nm MoO_x and PEDOT:PSS as a function of storage time in air under ambient conditions. The MoO_x based BHJ solar cells without encapsulation exhibit better air stability than PEDOT:PSS based ones. MoO_x based devices retain about 50 % of its original PCE after storage in air for 720 h, on the contrary, PEDOT:PSS based devices keep about 10 % of its original PCE after storage in air for 480 h, indicating that the former ones (MoO_x) have a slower degradation than the latter ones (PEDOT:PSS). The improvement of device stability is explained by the hygroscopic and acidic PSS, a source of interface instability due to the diffusion of PSS to other layers and reaction with other components. The replacement of PEDOT:PSS with MoO_x overcomes interface instability and yields significant improvement in air stability.

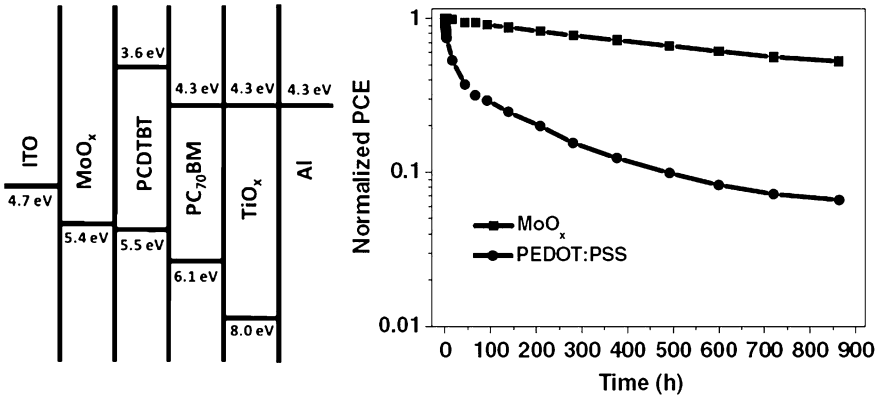

Fig. 6.12 (*left*) The device structure; (*right*) Normalized PCEs as a function of storage time for PCDTBT:PC_{70}BM solar cells fabricated with PEDOT:PSS and MoO_x in air under ambient conditions (no encapsulation) [72]. (Copyright John Wiley and Sons. Reproduced with permission)

6.4.2 Device Structures

6.4.2.1 Normal Structure

In normal structure, interface engineering can be concluded to improve the interface stability as discussed in Sect. 6.4.1.

6.4.2.2 Inverted Structure

A typical normal structure of OPV device is ITO/PEDOT:PSS/photoactive layer/LWF metal. LWF metal as cathode is a primary limit to the interface stability of devices since LWF metals (Li, Ca, and Al) are prone to be oxidized, resulting in the increase of series resistance at the organic/electrode interface and degrading device performance. In addition, oxygen preferably diffuses into the photoactive layer through pinholes and grain boundaries through the cathode, degrading the active layer and making the device instable in air [4]. On the other hand, the ITO/PEDOT:PSS interface is also instable due to likely indium diffusion into the photoactive layer and the ITO etching by acidic PEDOT:PSS adsorbing water [6, 51]. The reaction between PSS and water induces a faster degradation of the ITO/PEDOT:PSS interface [6].

To overcome the instability issue in normal structure device, one feasible approach is to construct an inverted configuration [73], where ITO serves as the cathode and a high work-function (HWF) metal as the anode, as shown in Fig. 6.13. It should be pointed out that only modified ITO can serve as the cathode for electron extraction. The functional layers for modifying ITO mainly focus on metal oxides such as TiO_2 [74] and ZnO [75, 76], and alkali-metal compound like

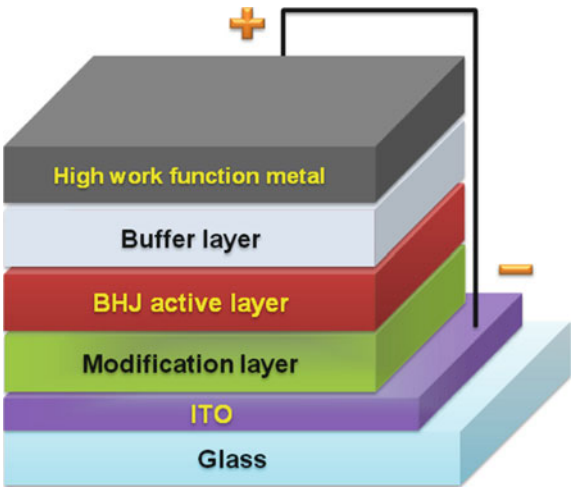

Fig. 6.13 A typical inverted device structure

Cs_2CO_3 [77, 78]. Large-area inverted devices with ZnO can also be realized by roll-to-roll processing of each layer [21, 79–81].

In principal, the inverted structure offers higher air stability than the normal one due to relatively stable HWF metal as top anode. Sahin et al. demonstrated a more air-stable inverted device with a structure of ITO/Perylene/MEH-PPV:PCBM/CuPc/Au than a normal device [82]. The inverted device shows a PCE of 0.14 % under 74.5 mW/cm^2 illumination in the first day. Although oxygen and humidity are present, the PCE is decreased by 27 % of the initial value after 2 weeks. On the contrary, the normal device with LiF/Al as top cathode has a PCE of 1.3 % under 100 mW/cm^2 illumination; however, the efficiency decreases by 91 % after only 1 day during storage in oxygen and diminishes thoroughly after a few days in air.

Hau et al. conducted the air-stability study of inverted devices employing ZnO nanoparticles (NP) as an electron-transporting layer and PEDOT:PSS/Ag as a hole-transporting layer and top anode [83]. The shelf lifetime is defined as the time when the PCE drops to half of its initial value. Figure 6.14a shows the *J–V* curves of a normal device of ITO/PEDOT:PSS/P3HT:PCBM/LiF/Al over variable periods from 0 to 4 days. The results show that the shelf lifetime is only 1 day, and a complete degradation is followed after 4 days. A large reduction of dark current at 2 V is observed after 4 days, as shown in the inset of Fig. 6.14a, suggesting the increased series resistance to be part of the degradation mechanism. On the other hand, the inverted device with a structure of ITO/ZnO NP/P3HT:PCBM/PEDOT:PSS/Ag without encapsulation exhibits a relatively stable performance despite being kept in air for a long time. A 20 % decrease of PCE is shown in Fig. 6.14b after 40 days. It is interesting that the decrease of dark current after a long-time storage does not occur.

Similarly, Liu et al. reported the stability improvement of inverted small-molecule OPVs with a structure of ITO/ZnO/CuPc:C_{60}/CuPc/PEDOT:PSS/Ag [84]. The authors compare two measurements for device stability: one is to test

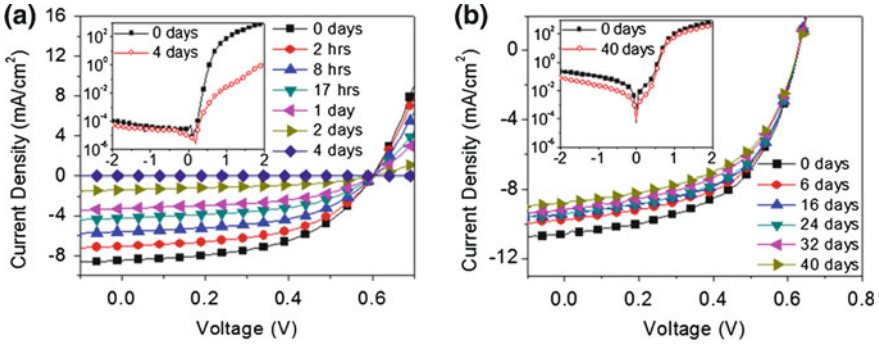

Fig. 6.14 *J–V* characteristics of unencapsulated **a** normal device over a period of 4 days and **b** inverted device over a period of 40 days in air under ambient conditions. Inset: dark *J–V* characteristics of the respective devices [83]. (Reprinted with permission from Ref. [83]. Copyright [2008], American Institute of Physics)

shelf lifetime (devices are kept in the dark), which is 912 h for inverted devices and 256 h for normal ones; meanwhile the other one is that the devices are kept under 100 mW/cm^2, exhibiting a negligible degradation for inverted devices and a faster degradation for normal devices due to continuous illumination. The stability tests imply that the degradation rate for inverted devices is slower than that for normal devices.

Such stability improvement could also be achieved by using TiO_x as the modification layer for ITO. Kuwabara et al. compared the stability of P3HT:PCBM-based inverted and normal devices with a structure of ITO/TiO_x/P3HT:PCBM/PEDOT:PSS/Au and ITO/PEDOT:PSS/P3HT:PCBM/Al, respectively. The devices were measured in ambient atmosphere under 100 mW/cm^2 [85]. As shown in Fig. 6.15, the PCE of the normal device drops to 50 % of its initial value after continuous illumination for 10 h, and the inverted device without encapsulation keeps its initial efficiency for 20 h under continuous illumination, indicating good stability either in ambient environment or under continuous illumination for inverted devices.

As an alternative, modifying ITO by a LWF metal would be an effective and simple approach to lower the work function of ITO. On the other hand, the contact between anode and active layer should be significantly improved by a buffer layer such as PEDOT:PSS [86], V_2O_5 [67, 73], and WO_3 [87] in order to reduce the exciton quenching and then increase the charge collection efficiency. Except for the roles of hole transport and extraction, such an anode buffer layer also acts as an optical spacer, adjusting the effective optical field distribution [88]. More importantly, the interface stability could be enhanced due to the prevention of oxygen and moisture from diffusing to active layer by using transition metal oxides (MoO_3 and V_2O_5).

Zimmermann et al. [89] systematically investigated the long-term stability of P3HT:PCBM-based OPVs with an inverted structure, as shown in Fig. 6.16, where

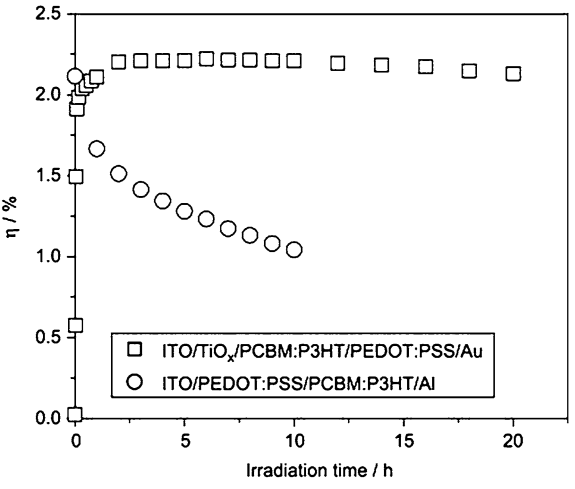

Fig. 6.15 The variation in η (PCE) of inverted device (ITO/TiOx/P3HT:PCBM/PEDOT:PSS/Au) and conventional device (ITO/PEDOT:PSS/P3HT:PCBM/LiF/Al) with irradiation time [85]. (Reprinted from [85], with permission from Elsevier) (http://www.sciencedirect.com/science/journal/09270248)

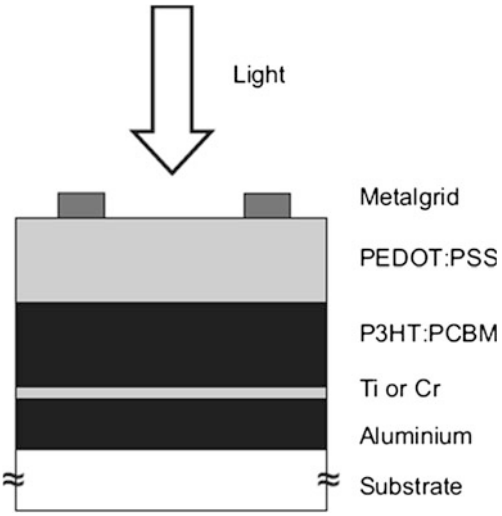

Fig. 6.16 Schematic structure of the inverted device. The first layer deposited on the substrate is the metallic electron contact, followed by the P3HT:PCBM blend and the PEDOT:PSS hole contact. The current is collected by a metal grid [89]. (Reprinted from [89], with permission from Elsevier) (http://www.sciencedirect.com/science/journal/09270248)

the devices consist of two different electron contact materials, titanium (Ti) and chromium (Cr), and two different thicknesses of P3HT:PCBM layers. In order to get the information of chemical composition distribution at the interface of active layer and metallic electron contact, Auger electron spectroscopy (AES) has been employed to show that electron contact is partially oxidized during the fabrication of inverted devices. It is concluded that oxygen is chemically bound at the organic/metal interface as well for Ti as for Cr as a contact layer. Moreover, both electrode material and active layer thickness have influences on the long-term stability of P3HT:PCBM BHJ inverted OPVs, and their results indicate that the devices with Cr as electrode are much more stable than those with Ti as electrode and a thinner active layer also has a positive effect. Two possibilities are to explain the effect of the layer thickness: one is that lower photocurrent caused by thinner active layers induces lower voltage drop due to the increase in series resistance caused by the decreased conductivity of PEDOT:PSS during aging [89, 90]; the other one is that defects in active layer affect and reduce the FF, especially for thick layers [89, 91]. After 1500 h of continuous illumination under a sulfur plasma lamp (100 mW/cm^2) at 50 °C, the most stable devices maintain 90 of their initial efficiency of more than 2.5 %. The results indicate that inverted structure is beneficial to the device stability.

We have presented inverted OPVs with LWF metals as interfacial layer modifying ITO as cathode [92–94]. First, we have investigated the impact of an ultrathin Ca deposited by thermal evaporation in inverted cell using a structure of ITO/Ca/P3HT:PCBM/MoO_3/Ag (Fig. 6.17 (left)) [94]. With the use of Ca lowering the work function of ITO and MoO_3 modifying the Ag anode, the efficiency of inverted devices is significantly improved compared with those without either of these two interfacial layers. Since Ca modifying the ITO is easily oxidized, we fabricated a CaO modified ITO on purpose to check if the corresponding device

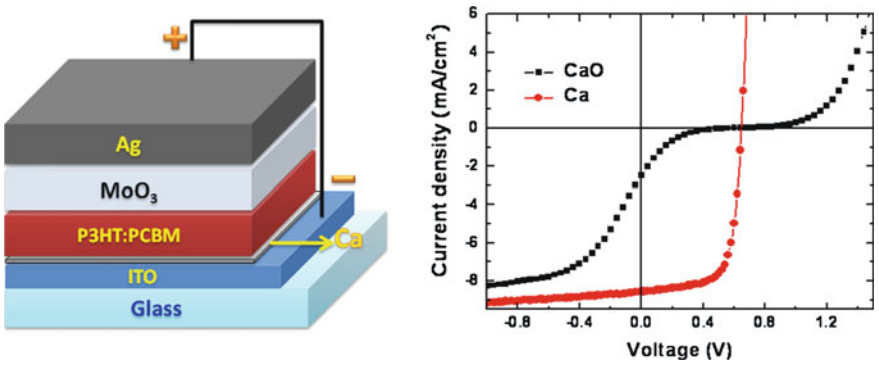

Fig. 6.17 (*left*) Device structure of an inverted OPV; (*right*) I–V characteristics of the devices with CaO and Ca as the electron-transporting layers under 100 mW/cm^2 illumination [92]. (Reprinted from [92], with permission from Elsevier) (http://www.sciencedirect.com/science/journal/09270248)

can still work properly. The CaO layer was obtained by purposely oxidizing the Ca deposited (expose the Ca to dry air). All the other layers are exactly the same. Figure 6.17 (right) shows the comparison of the *I–V* characteristics of two devices with the structures of ITO/Ca/P3HT:PCBM/MoO_3/Ag and ITO/CaO/P3HT:PCBM/MoO_3/Ag under 100 mW/cm^2. It is obvious that the device with CaO exhibits rather poor performance compared to that with Ca. In this way, we can indirectly confirm that Ca is not oxidized (at least not fully oxidized). Therefore, it can be concluded that the Ca still primarily remains in its metallic state.

Moreover, we have compared the effect of various metals (Ca, Mg, Al, and Ag) on electron collection. The results indicate that Ca and Mg give comparable photovoltaic effect. By comparison of inverted and normal devices, the improvement of the efficiency for inverted devices is explained by the possible origin from the favored vertical composition gradient of the P3HT:PCBM layer for the inverted device. It was reported that the active layer of P3HT:PCBM fabricated by spin-coating and post-annealing process usually has a composition with a higher PCBM (electron acceptor) content close to the substrate and a higher P3HT (electron donor) content close to the free (air) surface [73, 95]. This vertical composition gradient has an adverse effect on the photovoltaic performance of a normal forward device using glass/ITO/PEDOT:PSS as the bottom anode. However, this composition gradient is favorable to our inverted device because a P3HT-rich donor phase on the hole collecting side (MoO_3/Au) and a PCBM-rich acceptor phase on the electron collecting side (ITO/Ca) would reduce the charge recombination at the electrodes [96]. In addition, the possible metal penetration or damage to the active layer, caused by the deposition of the top metal contact [97], can be prevented in the inverted structure due to the protection of MoO_3 layer.

It is worth mentioning that all devices were not encapsulated for the measurement of air stability. The air stability of the inverted device is significantly

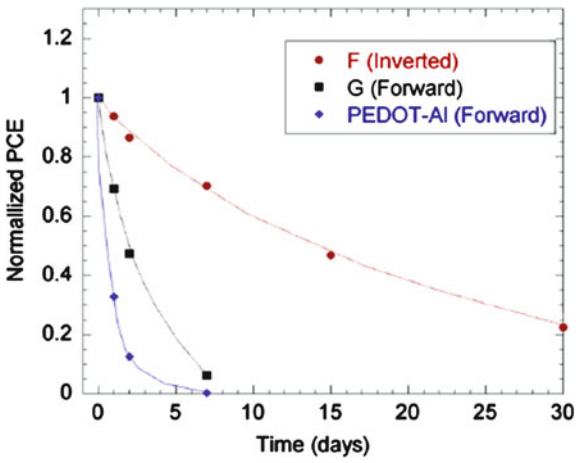

Fig. 6.18 Air-stability of the inverted and forward cells [93]. (Reprinted from [93], with permission from Elsevier) (http://www.sciencedirect.com/science/journal/09270248)

improved as compared with that of the normal device [93]. Figure 6.18 shows the change in the normalized PCE against the air-exposure time for inverted and normal OPVs. It is observed clearly that the shelf lifetime of the inverted device F is ~15 days, however the shelf lifetime of the normal cell G is only ~2 days. The explanation for the improvement of air stability for the inverted cell can be as follows. In the normal device G (ITO/MoO_3(10 nm)/P3HT:PCBM/Ca(10 nm)/Ag), the LWF metal (Ca) cathode on top of the active layer would easily react with the water and oxygen in air although a layer of Ag is deposited on top of the Ca layer. On the contrary, in the inverted device F (ITO/Ca(1 nm)/P3HT:PCBM/MoO_3(10 nm)/Au), air-stable Au is used as the top anode, however the reactive Ca incorporated between ITO and P3HT:PCBM layer has been prevented from its direct contact with air, resulting in the improvement of air stability. Figure 6.18 also shows the degradation of a normal PEDOT-Al device (ITO/PEDOT/P3HT:PCBM/Al) with time for comparison, which presents the poorest air stability with a short shelf lifetime of ~0.5 day. The rapid degradation of the PEDOT-Al cell can be ascribed to the degradations of both organic/Al and ITO/PEDOT interfaces [28, 98]. Therefore, the results reveal that LWF metals are also suitable to be adopted as electron selective interfacial layer for inverted cell and good for stability improvement.

6.4.3 Device Encapsulation

As discussed before, OLEDs suffer from different modes of degradations as (i) dark-spot degradation, (ii) catastrophic failure, and (iii) intrinsic degradation. The first two modes of degradation could be effectively controlled by means of proper device encapsulation and adequate control over device fabrication conditions; meanwhile, the intrinsic degradation mode has been far more challenging and continues to be an issue for OLED commercialization [20, 31, 32].

In OPV devices, PPV and its derivatives have been used, however, these polymers based devices exhibit low stability under illumination in air. Hence, an alternative is to use the polythiophenes, such as P3HT, which has given a PCE of 5 % or higher [99–101]. At the same time, the lifetime is reported in the range of 1000 h [102]. Very long-lifetime devices based on P3HT have also been presented with accelerated lifetime testing for 4000 h or even more than 1 year [103, 104]. It is thought that accelerated testing for 1 year corresponds to an operational lifetime of 3–10 years [37, 104].

Such a long lifetime would bring the technology into an expectation that this should be commercialized in the near future. However, one of the significant concerns or big challenges about commercialization is the stable encapsulation scheme for OPV devices. It is known that OPVs exhibit a rather poor property of air stability due to the chemical and physical and even mechanical degradations, primarily resulting from the oxygen and moisture in the atmosphere. Except for the stability improvements in essential materials and device structures, it is necessary and important to develop the technology and approaches of the device encapsulation benefiting to the long lifetime of OPV operation. Therefore, adequate encapsulation from ambient oxygen and water is an essential requirement for the commercial viability of OPV cells. The encapsulating layer in turn should be thin, defect-free, light weight, and offer ease of processing [105].

In this section, we will discuss a few methods on encapsulation techniques and their effect on the device stability.

Krebs et al. presented P3HT:PCBM-based device with an operational stability for more than a year after an efficient and proper method for the encapsulation, exhibiting a decrease in the efficiency to 65 % compared to the initial value [104]. This method follows the process of (1) device preparation on glass substrates; (2) sealing by using glass fiber reinforced thermosetting epoxy against a back plate. Such an encapsulation makes it possible to transport oxygen and moisture sensitive OPV devices outside a glove box. The author emphasized that once the substrates, backplate, prepreg, and jig are available in laboratory, this fast and simple sealing procedure requires only 10 min of work besides the thermosetting time of 12 h.

Atomic layer deposition (ALD) is a chemical vapor deposition technique involving the cycling of alternate precursor gasses into a chamber to react on the surface of samples and grow high-quality and conformal films [106, 107]. Ultrathin barrier layers have become promising candidates for device encapsulation [105, 107, 108], which are deposited by ALD at low temperature, particularly suitable for organic and flexible electronics as passivation layers with excellent film conformity [105].

Chang et al. presented a thin-film encapsulation of Al_2O_3/HfO_2 for OPVs by using ALD [108], in which 26 nm Al_2O_3/HfO_2 nanolaminated films consist of 52 pairs of alternating 2 Al_2O_3 and 3 HfO_2 layers, and the deposition temperature is 140 or 150 °C, and the chamber pressure is 0.1 Torr. Encapsulating the devices with ALD films brings three problems of ALD films: (1) poor nucleation on the surface of P3HT:PCBM layer exposed at the device edges, resulting in incomplete coverage of the ALD films (Fig. 6.19b); (2) rapid hydrolysis in air, causing the

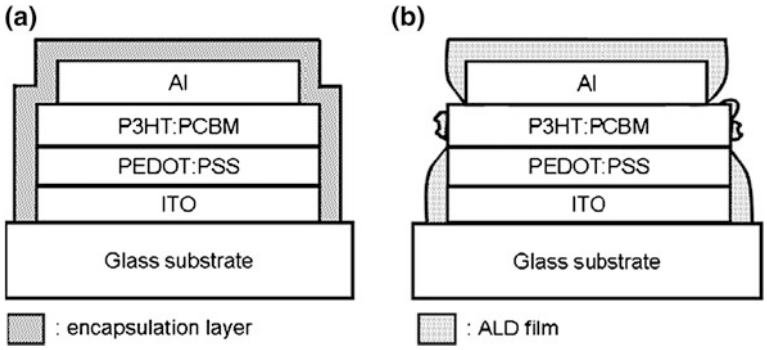

Fig. 6.19 Schematics of the cross-section of the PV devices: **a** Encapsulated by a barrier film with complete coverage over all device surface and **b** Encapsulated by a barrier film that has poor surface coverage over the P3HT/PCBM layer [108]. (Reprinted from [108], with permission from Elsevier) (http://www.sciencedirect.com/science/journal/15661199)

encapsulating films to disintegrate as the devices aged; (3) susceptibility to mechanical damages during device characterization and handling. The Al_2O_3/HfO_2 nanolaminated structure can overcome the issue of hydrolysis-induced aging for only Al_2O_3 films, owing to the hydrophobicity of the HfO_2 layers. However, a UV-curable epoxy resin film as a capping layer is required for the Al_2O_3/HfO_2 encapsulation of the devices in order to reach the control of the degradation profile. The aims to use this capping layer are (1) to reduce the accidental damages during characterization and handling due to its thin thickness and also to enhance the mechanical protection; (2) to diminish the small defects in the ALD film due to the hydrophobicity of the P3HT:PCBM surface. This technique can prevent device degradation induced by ambient atmosphere and also play a role in annealing step beneficial to the increase of the initial efficiency. Figure 6.19 shows the comparison of two devices encapsulated by a barrier film with complete coverage over all device surface and poor coverage over the P3HT:PCBM layer, indicating the importance of complete coverage surface for stability improvement. When the ALD temperature is fixed at 140 °C and the deposition time is 1 h, the devices achieve a PCE of 3.66 % due to optimal annealing during encapsulation.

As shown in Fig. 6.20, Potscavage et al. developed a 200 nm Al_2O_3 barrier layer grown by ALD as the encapsulation layer in pentacene/C_{60} based small-molecule OPVs [107]. The encapsulated device maintains a stable efficiency when exposed to ambient atmosphere for over 6000 h, much longer than those without encapsulation having a fast degradation upon exposure to air for 10 h. Moreover, the thermal annealing during ALD deposition improves the V_{oc} and then the overall PCE of the devices.

Figure 6.21 compares the change of main parameters of OPVs with various encapsulations from the initial values after exposure to ambient atmosphere, i.e., no encapsulation, UV epoxy, Al_2O_3, and Al_2O_3/UV epoxy. The device with no encapsulation degrades very fast, whose J_{sc} drops to <20 % of its initial value.

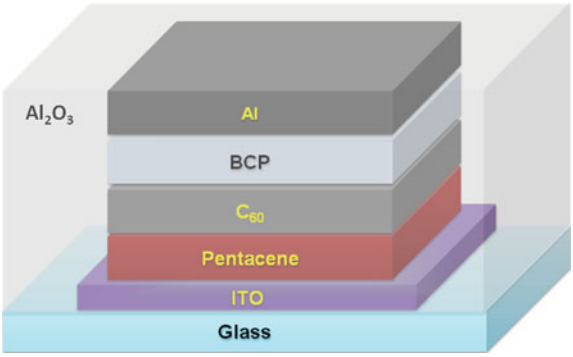

Fig. 6.20 Schematic of device structure [107]

The device encapsulated with only UV epoxy degrades by a slower rate, whose performance decreases to 50 % of the initial value after 100 h and to 25 % after almost 250 h upon exposure to ambient atmosphere due to a short-term protection of epoxy. The devices with Al_2O_3 by ALD and with or without UV epoxy layer have PCE and J_{sc} within 6 % of their initial values after 6,145 h of exposure to ambient atmosphere.

Moreover, Sarkar et al. did not use the UV-curable epoxy and developed improved ultrathin Al_2O_3 layers, grown by using ALD, as primary barrier layers for encapsulation of OPV devices [105], as shown in Fig. 6.22. The encapsulation characteristics of this barrier layer can be improved by replacing H_2O with O_3 as the ALD oxidant, exhibiting superior device encapsulation to the barrier layer grown by using H_2O. This Al_2O_3 barrier layer was done without any additional UV-curable epoxy resin film as a sealant for protecting the devices from ambient moisture and oxygen. Through optimization, the optimal thickness of Al_2O_3 is 18 nm to function well, and thus 210 cycles of O_3–Al_2O_3 give the best device encapsulation exhibiting 80 % of its initial efficiency over a period of 500 h. The authors have compared two different ALD temperatures functioning as an annealing step beneficial to the formation of phase separation in the active layer.

Additionally, Luo et al. presented a thin layer of MnO inserted in between photoactive layer and metal cathode to improve the device efficiency and air stability [109]. The results indicate that MnO can serve as electron-transporting layer and protection layer from damages caused by moisture and oxygen. The OPV device with 3 nm MnO layer retains a PCE of 28.42 % of its initial value after 2 weeks while the device without MnO layer has only 6.03 % of initial PCE just after 2 days without encapsulation. It is promising to use such a MnO layer to enhance both device efficiency and operation stability.

The most common technique to obtain an ultra-high barrier layer is to use alternating organic–inorganic multilayer, i.e., inserting inorganic barriers between polymer buffers to reduce the number of pinholes [110], resulting in smoothly coated surface, decreased mechanical damage, and increased thermal stability [18]. On the other hand, stacked structure is produced by repeating the alternating process, allowing organic layers to “decouple” the defects from neighboring inorganic layers. Madakasira et al. reported the conformal deposition of parylene

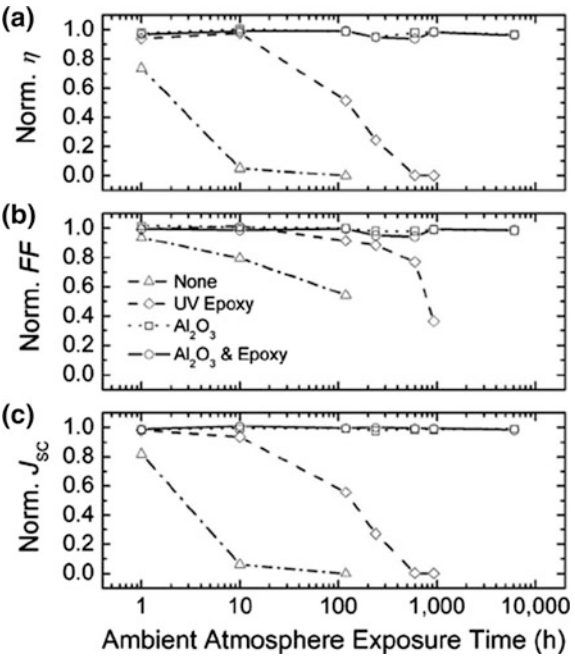

Fig. 6.21 Relative change in **a** η, **b** FF, and **c** J_{sc} of solar cells with various types of encapsulation from the initial values after exposure to ambient atmosphere. Four devices are shown with the following types of encapsulation: no encapsulation (dash-dotted line, *triangle*); UV epoxy (*dashed line*, *diamond*); Al_2O_3 (*dotted line*, *square*); and Al_2O_3 and UV epoxy (*solid line*, *circle*). The values for each device are normalized to the initial value for that device [107]. (Reprinted with permission from Ref. [107]. Copyright [2007], American Institute of Physics)

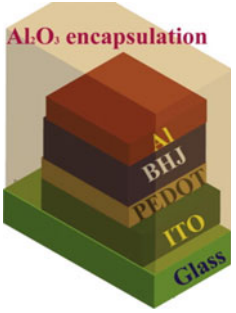

Fig. 6.22 Schematics of the device structure encapsulated with Al_2O_3. BHJ is P3HT:PCBM [105]. (Reprinted from [105], with permission from Elsevier) (http://www.sciencedirect.com/science/journal/15661199)

on polymer OPVs [111]. The results show that single parylene coating layer is not efficient to protect the degradation of P3HT:PCBM-based devices due to its photochemical reactions caused by oxygen. More importantly, the authors develop multilayer barriers consisting of parylene and Al_2O_3 to implement the full protection of the devices from degrading even under illumination.

It is promising that Dennler et al. firstly studied the shelf lifetime of MDMO-PPV:PCBM-based OPVs encapsulated by flexible and transparent ultra-high barrier poly(ethylene naphthalate) (PEN) grown by plasma enhanced chemical vapor deposition (PECVD) [19]. Figure 6.23 shows the cross-sectional view of OPV device and a photo of a bent device. Such an encapsulation could improve the shelf lifetime of OPV device with 30×57 mm^2 from a few hours to the range beyond 3000 h.

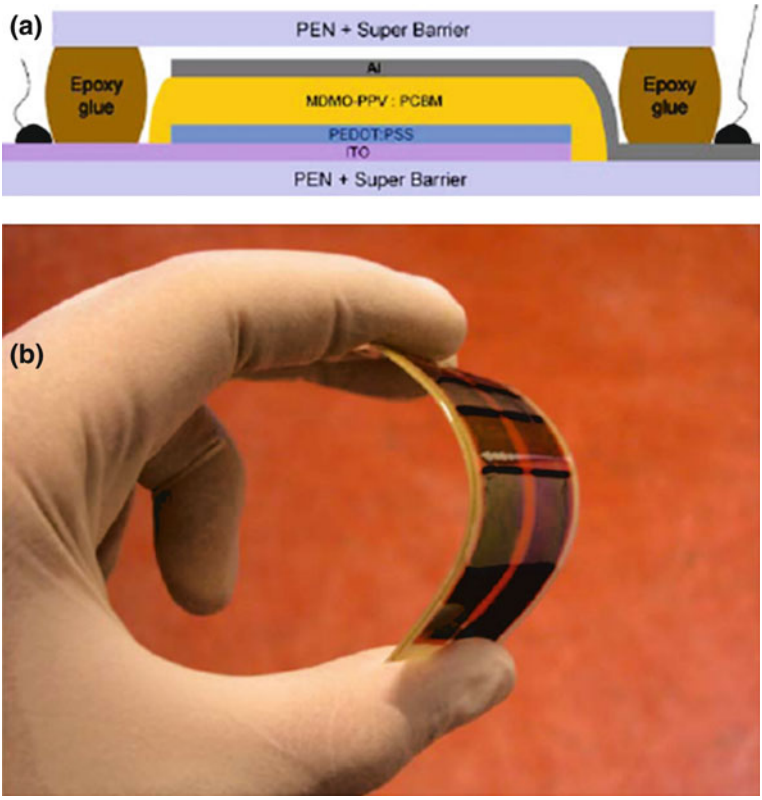

Fig. 6.23 **a** Cross-sectional view of the OPV device; **b** Picture of a bent device [19]. (Reprinted from [19], with permission from Elsevier) (http://www.sciencedirect.com/science/journal/00406090)

6.5 Conclusion and Outlook

6.5.1 Conclusion

With the rapid progress predominantly in the achievements of material science, the efficiency of OPVs has boosted significantly to the aim of industrial products. Low cost and long lifetime are also initially required by the market.

The degradation mechanisms of interface stability in OPVs have been presented, which are closely correlated with electrodes materials and interfacial layers modifying the electrode/organic interface due to the diffusion of oxygen and water into these layers and also their intrinsic properties.

In order to well understand the mechanisms, highly effective characterization techniques are of great significance to monitor and analyze the origins of interface instability and the degree of their influence. These characterization techniques, in

view of optical and electrical properties, provide various information of the changes of electronic/chemical structure, energy level, and energy/charge transfer at the interface.

All efforts on analyzing interface degradation mechanism and exploiting characterization techniques are serving as pathways toward further optimization and improvement of interface stability and device stability, such as essential materials used, device design and structure, and encapsulation, significantly crucial for the technological applications.

6.5.2 Outlook

If organic semiconducting and metallic materials and device design were further developed, it is much promising that efficiencies of 10 would be obtained in a relatively short term since 8 % efficiency has already been achieved by many companies so far. The future of renewable and green OPV technology turns out to be bright.

Another important factor is economical, i.e., to address the balance of product cost, which demands the progress of technology such as new electrodes' alternative to current ITO and metals, cost-reduced synthesis process of photoactive materials, low-cost encapsulation against oxygen and moisture diffusion, and fabrication process of flexible cells and flexible integrated power supply.

The last requirement for commercial technology of OPVs is lifetime or stability. High sensitivity to moisture, oxygen, UV light, and temperature results in serious degradations of organic materials and entire devices. In order to diminish the instability and extend the device lifetime, deep understanding and investigation on degradation of each component and interface via chemical and physical ways are necessary, followed by improvement techniques. Therefore, study of degradation is suggested as follows:

6.5.2.1 Electrodes

ITO as highly conductive and transparent anode faces problems of lack of indium reserves in nature and damage of indium to organic layer via diffusion. PEDOT:PSS as anode buffer layer exhibits slight acid property after adsorbing water, leading to the etched ITO. Thus, an alternative to ITO is gallium doped ZnO (GZO) which has a proper work function as anode and air stability. A replacement of hydrophilic and acidic PEDOT:PSS with metal oxides is viable since metal oxides with hole-transporting behavior as anode buffer layer exhibit appropriate work functions and stability against air. However, most of metal oxides are grown under high vacuum, which raises the process cost and hinders the large area. Therefore, solution-processed metal oxides as buffer layers could provide many opportunities and important insights on commercial OPVs.

LWF metals as cathode are easily oxidized, causing dark spots and degrading devices very fast. One way is to use inverted structure as mentioned before. The other way is to develop advanced encapsulation technology to protect the devices from moisture and oxygen.

6.5.2.2 Photoactive Materials

Organic semiconductors are easily oxidized by oxygen, especially under illumination. However, OPVs must be exposed to solar light during operation. Therefore, it is challenging to synthesize and develop air-stable organic materials with deep HOMO levels and low band gaps.

6.5.2.3 Device Design

BHJ structure offers an interpenetrating network for charge transport, which is controlled by annealing, solvents, additives, etc. The morphology is changeable by varying the annealing temperature and processing time, i.e., not at the thermodynamic equilibrium. Thus, it is necessary to exploit an effective and stable morphology beneficial to both efficiency and stability, providing bi-continuous pathways for charge transport in their individual phase. More importantly, it should be temperature and light stable, especially under illumination when the device is heated up.

On the other hand, inverted structure facilitates the stability improvement due to the reverse of anode and cathode, where HWF metal as anode at top could sustain the oxidization.

6.5.2.4 Encapsulation

Low-cost encapsulation technology leads to limited protection against oxygen and water. Therefore, a proper and powerful encapsulation is necessary to further improve the device stability. Encapsulation of alternating inorganic–organic multilayer actually serves as a high barrier, fulfilling the requirements for flexible OPVs. The encapsulating layer should be possessed with easy process, light weight, no defects, and flexibility.

In summary, all the factors influencing device stability should be emphasized in order to prolong device lifetime and achieve commercial products. Taking various interface parameters and factors into account, a much more comprehensive model should be established by improving previous models mentioned before. Deep insight and knowledge into degradation mechanism, which could disclose the relationship between degradation mechanisms and material design, preparation technique, heat effect during operation, annealing treatment, and encapsulation, are significantly beneficial to optimization of organic material design and device stability.

References

1. Konarka Technologies I http://www.konarka.com/
2. Heliatek G http://www.heliatek.com/
3. Solarmer Energy I http://www.solarmer.com/
4. Cai WZ, Gong X, Cao Y (2010) Polymer solar cells: recent development and possible routes for improvement in the performance. Sol Energy Mater Sol Cells 94:114–127
5. Helgesen M, Sondergaard R, Krebs FC (2010) Advanced materials and processes for polymer solar cell devices. J Mater Chem 20:36–60
6. Liang YY, Xu Z, Xia JB et al (2010) For the bright future-bulk heterojunction polymer solar cells with power conversion efficiency of 7.4 %. Adv Mater 22:E135–E138
7. Dennler G, Scharber MC, Brabec CJ (2009) Polymer-fullerene bulk-heterojunction solar cells. Adv Mater 21:1323–1338
8. Jorgensen M, Norrman K, Krebs FC (2008) Stability/degradation of polymer solar cells. Sol Energy Mater Sol Cells 92:686–714
9. Shrotriya V http://www.slideshare.net/vshrotriya/organic-solar-cells
10. Padinger F, Fromherz T, Denk P et al (2001) Degradation of bulk heterojunction solar cells operated in an inert gas atmosphere: a systematic study. Synth Met 121:1605–1606
11. Neugebauer H, Brabec C, Hummelen JC et al (2000) Stability and photodegradation mechanisms of conjugated polymer/fullerene plastic solar cells. Sol Energy Mater Sol Cells 61:35–42
12. Jeranko T, Tributsch H, Sariciftci NS et al (2004) Patterns of efficiency and degradation of composite polymer solar cells. Sol Energy Matter Sol Cells 83:247–262
13. Kroon JM, Wienk MM, Verhees WJH et al (2002) Accurate efficiency determination and stability studies of conjugated polymer/fullerene solar cells. Thin Solid Films 403:223–228
14. Krebs FC, Alstrup J, Spanggaard H et al (2004) Production of large-area polymer solar cells by industrial silk screen printing, lifetime considerations and lamination with polyethyleneterephthalate. Sol Energy Matter Sol Cells 83:293–300
15. Krebs FC, Carle JE, Cruys-Bagger N et al (2005) Lifetimes of organic photovoltaics: photochemistry, atmosphere effects and barrier layers in ITO-MEHPPV: PCBM-aluminium devices. Sol Energy Matter Sol Cells 86:499–516
16. Brabec CJ, Hauch JA, Schilinsky P et al (2005) Production aspects of organic photovoltaics and their impact on the commercialization of devices. MRS Bull 30:50–52
17. Holdcroft S (1991) Photochain scission of the soluble electronically conducting polymer—Poly(3-Hexylthiophene). Macromolecules 24:2119–2121
18. Lewis JS, Weaver MS (2004) Thin-film permeation-barrier technology for flexible organic light-emitting devices. IEEE J Sel Top Quantum Electron 10:45–57
19. Dennler G, Lungenschmied C, Neugebauer H et al (2006) A new encapsulation solution for flexible organic solar cells. Thin Solid Films 511:349–353
20. Aziz H, Popovic ZD (2004) Degradation phenomena in small-molecule organic light-emitting devices. Chem Mater 16:4522–4532
21. Krebs FC, Gevorgyan SA, Alstrup J (2009) A roll-to-roll process to flexible polymer solar cells: model studies, manufacture and operational stability studies. J Mater Chem 19: 5442–5451
22. Norrman K, Gevorgyan SA, Krebs FC (2009) Water-induced degradation of polymer solar cells studied by (H2O)-O-18 labeling. Acs Appl Mater Interfaces 1:102–112
23. Norrman K, Madsen MV, Gevorgyan SA et al (2010) Degradation patterns in water and oxygen of an inverted polymer solar cell. J Am Chem Soc 132:16883–16892
24. Scott JC, Kaufman JH, Brock PJ et al (1996) Degradation and failure of MEH-PPV light-emitting diodes. J Appl Phys 79:2745–2751
25. Carter SA, Angelopoulos M, Karg S et al (1997) Polymeric anodes for improved polymer light-emitting diode performance. Appl Phys Lett 70:2067–2069

26. Krebs FC, Norrman K (2007) Analysis of the failure mechanism for a stable organic photovoltaic during 10000 h of testing. Prog Photovolt Res Appl 15:697–712
27. Brabec C, Dyakonov V, Parisi J, et al (2003) Organic photovoltaics: concepts and realization, p 60
28. de Jong MP, van Ijzendoorn LJ, de Voigt MJA (2000) Stability of the interface between indium-tin-oxide and poly(3,4-ethylenedioxythiophene)/poly(styrenesulfonate) in polymer light-emitting diodes. Appl Phys Lett 77:2255–2257
29. Girtan M, Rusu M (2010) Role of ITO and PEDOT:PSS in stability/degradation of polymer: fullerene bulk heterojunctions solar cells. Sol Energy Matter Sol Cells 94:446–450
30. Kawano K, Pacios R, Poplavskyy D et al (2006) Degradation of organic solar cells due to air exposure. Sol Energy Matter Sol Cells 90:3520–3530
31. Aziz H, Xu G (1996) A degradation mechanism of organic light-emitting devices. Synth Met 80:7–10
32. Aziz H, Popovic ZD, Hu NX et al (1999) Degradation mechanism of small molecule-based organic light-emitting devices. Science 283:1900–1902
33. Reese MO, Morfa AJ, White MS et al (2008) Pathways for the degradation of organic photovoltaic P3HT : PCBM based devices. Sol Energy Matter Sol Cells 92:746–752
34. Reese MO, Morfa AJ, White MS et al (2008) Short-term metal/organic interface stability investigations of organic photovoltaic devices. Pvsc: 2008 33rd IEEE photovoltaic specialists conference. vols 1–4:1491–1493
35. Li JG, Kim S, Edington S et al (2011) A study of stabilization of P3HT/PCBM organic solar cells by photochemical active TiOx layer. Sol Energy Matter Sol Cells 95:1123–1130
36. Fery C, Racine B, Vaufrey D et al (2005) Physical mechanism responsible for the stretched exponential decay behavior of aging organic light-emitting diodes. Appl Phys Lett 87:213502
37. Schuller S, Schilinsky P, Hauch J et al (2004) Determination of the degradation constant of bulk heterojunction solar cells by accelerated lifetime measurements. Appl Phys A Mater Sci Process 79:37–40
38. Logdlund M, Bredas JL (1994) Theoretical-studies of the interaction between aluminum and poly(P-phenylenevinylene) and derivatives. J Chem Phys 101:4357–4364
39. Karst N, Bernede JC (2006) On the improvement of the open circuit voltage of plastic solar cells by the presence of a thin aluminium oxide layer at the interface organic/aluminium. Phys Status Solidi A-Appl Mat 203:R70–R72
40. Melzer C, Krasnikov VV, Hadziioannou G (2003) Organic donor/acceptor photovoltaics: the role of C-60/metal interfaces. Appl Phys Lett 82:3101–3103
41. Vogel M, Doka S, Breyer C et al (2006) On the function of a bathocuproine buffer layer in organic photovoltaic cells. Appl Phys Lett 89:163501
42. Zhang ST, Zhou YC, Zhao JM et al (2006) Role of hole playing in improving performance of organic light-emitting devices with an Al2O3 layer inserted at the cathode-organic interface. Appl Phys Lett 89:043502
43. Hung LS, Tang CW, Mason MG (1997) Enhanced electron injection in organic electroluminescence devices using an Al/LiF electrode. Appl Phys Lett 70:152–154
44. Brabec CJ, Shaheen SE, Winder C et al (2002) Effect of LiF/metal electrodes on the performance of plastic solar cells. Appl Phys Lett 80:1288–1290
45. van Gennip WJH, van Duren JKJ, Thune PC et al (2002) The interfaces of poly(p-phenylene vinylene) and fullerene derivatives with Al, LiF, and Al/LiF studied by secondary ion mass spectroscopy and x-ray photoelectron spectroscopy: formation of AlF3 disproved. J Chem Phys 117:5031–5035
46. McNeill CR, Fell CJR, Holdsworth JL et al (2005) Screening for artifacts in near-field scanning photocurrent microscopy images of polymer solar cells. Synth Met 153:85–88
47. Renaud G, Lazzari R, Leroy F (2009) Probing surface and interface morphology with grazing incidence small angle X-ray scattering. Surf Sci Rep 64:255–380
48. Caminiti R, Albertini VR (1999) The kinetics of phase transitions observed by energy-dispersive X-ray diffraction. Int Rev Phys Chem 18:263–299

49. Orita K, Morimura T, Horiuchi T et al (1997) In situ energy-dispersive X-ray reflectivity measurements of structural changes in thin films for organic electroluminescent devices. Synth Met 91:155–158
50. Paci B, Generosi A, Albertini VR et al (2005) In situ energy dispersive x-ray reflectometry measurements on organic solar cells upon working. Appl Phys Lett 87:194110
51. Paci B, Generosi A, Albertini VR et al (2006) Controlling photoinduced degradation in plastic photovoltaic cells: a time-resolved energy dispersive x-ray reflectometry study. Appl Phys Lett 89:043507
52. Andreasen JW, Gevorgyan SA, Schleputz CM et al (2008) Applicability of X-ray reflectometry to studies of polymer solar cell degradation. Sol Energy Matter Sol Cells 92:793–798
53. Garcia-Belmonte G, Munar A, Barea EM et al (2008) Charge carrier mobility and lifetime of organic bulk heterojunctions analyzed by impedance spectroscopy. Org Electron 9: 847–851
54. Bisquert J (2002) Theory of the impedance of electron diffusion and recombination in a thin layer. J Phys Chem B 106:325–333
55. Fabregat-Santiago F, Garcia-Belmonte G, Mora-Sero I et al (2011) Characterization of nanostructured hybrid and organic solar cells by impedance spectroscopy. Phys Chem Chem Phys 13:9083–9118
56. Garcia-Belmonte G, Boix PP, Bisquert J et al (2010) Simultaneous determination of carrier lifetime and electron density-of-states in P3HT:PCBM organic solar cells under illumination by impedance spectroscopy. Sol Energy Matter Sol Cells 94:366–375
57. Bisquert J, Fabregat-Santiago F, Mora-Sero I et al (2009) Electron lifetime in dye-sensitized solar cells: theory and interpretation of measurements. J Phys Chem C 113:17278–17290
58. Glatthaar M, Mingirulli N, Zimmermann B et al (2005) Impedance spectroscopy on organic bulk-heterojunction solar cells. Phys Status Solidi A-Appl Mat 202:R125–R127
59. Glatthaar M, Riede M, Keegan N et al (2007) Efficiency limiting factors of organic bulk heterojunction solar cells identified by electrical impedance spectroscopy. Sol Energy Mater Sol Cells 91:390–393
60. Wang MD, Xie FY, Xie WG et al (2011) Device lifetime improvement of polymer-based bulk heterojunction solar cells by incorporating copper oxide layer at Al cathode. Appl Phys Lett 98:183304
61. Wang MD, Tang Q, An J et al (2010) Performance and stability improvement of P3HT:PCBM-based solar cells by thermally evaporated chromium oxide (CrOx) interfacial layer. ACS Appl Mater Interfaces 2:2699–2702
62. Kim JY, Kim SH, Lee HH et al (2006) New architecture for high-efficiency polymer photovoltaic cells using solution-based titanium oxide as an optical spacer. Adv Mater 18:572–576
63. Kim JY, Lee K, Coates NE et al (2007) Efficient tandem polymer solar cells fabricated by all-solution processing. Science 317:222–225
64. Lee K, Kim JY, Park SH et al (2007) Air-stable polymer electronic devices. Adv Mater 19:2445–2449
65. Cho S, Lee K, Heeger AJ (2009) Extended lifetime of organic field-effect transistors encapsulated with titanium sub-oxide as an 'Active' passivation/barrier layer. Adv Mater 21:1941–1944
66. Lee JK, Coates NE, Cho S et al (2008) Efficacy of TiOx optical spacer in bulk-heterojunction solar cells processed with 1,8-octanedithiol. Appl Phys Lett 92:243308
67. Shrotriya V, Li G, Yao Y et al (2006) Transition metal oxides as the buffer layer for polymer photovoltaic cells. Appl Phys Lett 88:073508
68. Zhao DW, Sun XW, Jiang CY et al (2008) Efficient tandem organic solar cells with an Al/MoO3 intermediate layer. Appl Phys Lett 93:083305
69. Zhang F, Zhao D, Zhuo Z et al (2010) Inverted small molecule organic solar cells with Ca modified ITO as cathode and MoO3 modified. Sol Energy Matter Sol Cells 94:2416–2421

70. Zhang FJ, Sun FY, Shi YZ et al (2010) Effect of an ultra-thin molybdenum trioxide layer and illumination intensity on the performance of organic photovoltaic devices. Energy Fuels 24:3739–3742
71. Wang FX, Qiao XF, Xiong T et al (2008) The role of molybdenum oxide as anode interfacial modification in the improvement of efficiency and stability in organic light-emitting diodes. Org Electron 9:985–993
72. Sun Y, Takacs CJ, Cowan SR et al (2011) Efficient, air-stable bulk heterojunction polymer solar cells using moox as the anode interfacial layer. Adv Mater 23:2226–2230
73. Chen LM, Hong ZR, Li G et al (2009) Recent progress in polymer solar cells: manipulation of polymer: fullerene morphology and the formation of efficient inverted polymer solar cells. Adv Mater 21:1434–1449
74. Tao C, Ruan SP, Zhang XD et al (2008) Performance improvement of inverted polymer solar cells with different top electrodes by introducing a MoO3 buffer layer. Appl Phys Lett 93:193307
75. Hau SK, Yip HL, Ma H et al (2008) High performance ambient processed inverted polymer solar cells through interfacial modification with a fullerene self-assembled monolayer. Appl Phys Lett 93:233304
76. Kyaw AKK, Sun XW, Jiang CY et al (2008) An inverted organic solar cell employing a sol-gel derived ZnO electron selective layer and thermal evaporated MoO3 hole selective layer. Appl Phys Lett 93:221107
77. Li G, Chu CW, Shrotriya V et al (2006) Efficient inverted polymer solar cells. Appl Phys Lett 88:253503
78. Liao HH, Chen LM, Xu Z et al (2008) Highly efficient inverted polymer solar cell by low temperature annealing of Cs2CO3 interlayer. Appl Phys Lett 92:173303
79. Krebs FC (2009) All solution roll-to-roll processed polymer solar cells free from indium-tin-oxide and vacuum coating steps. Org Electron 10:761–768
80. Krebs FC (2009) Polymer solar cell modules prepared using roll-to-roll methods: Knife-over-edge coating, slot-die coating and screen printing. Sol Energy Mater Sol Cells 93:465–475
81. Krebs FC, Jorgensen M, Norrman K et al (2009) A complete process for production of flexible large area polymer solar cells entirely using screen printing-First public demonstration. Sol Energy Mater Sol Cells 93:422–441
82. Sahin Y, Alem S, de Bettignies R et al (2005) Development of air stable polymer solar cells using an inverted gold on top anode structure. Thin Solid Films 476:340–343
83. Hau SK, Yip HL, Baek NS et al (2008) Air-stable inverted flexible polymer solar cells using zinc oxide nanoparticles as an electron selective layer. Appl Phys Lett 92:253301
84. Liu JP, Wang SS, Bian ZQ et al (2009) Inverted photovoltaic device based on ZnO and organic small molecule heterojunction. Chem Phys Lett 470:103–106
85. Kuwabara T, Nakayama T, Uozumi K et al (2008) Highly durable inverted-type organic solar cell using amorphous titanium oxide as electron collection electrode inserted between ITO and organic layer. Sol Energy Mater Sol Cells 92:1476–1482
86. Steim R, Choulis SA, Schilinsky P et al (2008) Interface modification for highly efficient organic photovoltaics. Appl Phys Lett 92:093303
87. Tao C, Ruan SP, Xie GH et al (2009) Role of tungsten oxide in inverted polymer solar cells. Appl Phys Lett 94:043311
88. Ameri T, Dennler G, Waldauf C et al (2008) Realization, characterization, and optical modeling of inverted bulk-heterojunction organic solar cells. J Appl Phys 103:084506
89. Zimmermann B, Wurfel U, Niggemann M (2009) Longterm stability of efficient inverted P3HT:PCBM solar cells. Sol Energy Matter Sol Cells 93:491–496
90. Lee JK, Cho JM, Shin WS et al (2008) The stability of PEDOT: PSS films monitored by electron spin resonance. J Korean Phys Soc 52:621–626
91. Chang YM, Su WF, Wang L (2008) Influence of photo-induced degradation on the optoelectronic properties of regioegular poly(3-hexylthiophene). Sol Energy Matter Sol Cells 92:761–765

92. Zhao DW, Tan ST, Ke L et al (2010) Optimization of an inverted organic solar cell. Sol Energy Mater Sol Cells 94:985–991
93. Jiang CY, Sun XW, Zhao DW et al (2010) Low work function metal modified ITO as cathode for inverted polymer solar cells. Sol Energy Mater Sol Cells 94:1618–1621
94. Zhao DW, Liu P, Sun XW et al (2009) An inverted organic solar cell with an ultrathin Ca electron-transporting layer and MoO3 hole-transporting layer. Appl Phys Lett 95:153304
95. Campoy-Quiles M, Ferenczi T, Agostinelli T et al (2008) Morphology evolution via self-organization and lateral and vertical diffusion in polymer: fullerene solar cell blends. Nat Mater 7:158–164
96. Gunes S, Neugebauer H, Sariciftci NS (2007) Conjugated polymer-based organic solar cells. Chem Rev 107:1324–1338
97. Peumans P, Yakimov A, Forrest SR (2003) Small molecular weight organic thin-film photodetectors and solar cells. J Appl Phys 93:3693–3723
98. Wang EG, Wang L, Lan LF et al (2008) High-performance polymer heterojunction solar cells of a polysilafluorene derivative. Appl Phys Lett 92:033307
99. Li G, Shrotriya V, Huang JS et al (2005) High-efficiency solution processable polymer photovoltaic cells by self-organization of polymer blends. Nat Mater 4:864–868
100. Kim K, Liu J, Namboothiry MAG et al (2007) Roles of donor and acceptor nanodomains in 6% efficient thermally annealed polymer photovoltaics. Appl Phys Lett 90:163511
101. Reyes-Reyes M, Kim K, Carroll DL (2005) High-efficiency photovoltaic devices based on annealed poly(3-hexylthiophene) and 1-(3-methoxycarbonyl)-propyl-1-phenyl-(6,6)C-61 blends. Appl Phys Lett 87:083506
102. Yang XN, Loos J, Veenstra SC et al (2005) Nanoscale morphology of high-performance polymer solar cells. Nano Lett 5:579–583
103. Krebs FC, Spanggaard H (2005) Significant improvement of polymer solar cell stability. Chem Mat 17:5235–5237
104. Krebs FC (2006) Encapsulation of polymer photovoltaic prototypes. Sol Energy Mater Sol Cells 90:3633–3643
105. Sarkar S, Culp JH, Whyland JT et al (2010) Encapsulation of organic solar cells with ultrathin barrier layers deposited by ozone-based atomic layer deposition. Org Electron 11:1896–1900
106. Puurunen RL (2005) Surface chemistry of atomic layer deposition: a case study for the trimethylaluminum/water process. J Appl Phys 97:121301
107. Potscavage WJ, Yoo S, Domercq B et al (2007) Encapsulation of pentacene/C-60 organic solar cells with Al2O3 deposited by atomic layer deposition. Appl Phys Lett 90:253511
108. Chang CY, Chou CT, Lee YJ et al (2009) Thin-film encapsulation of polymer-based bulk-heterojunction photovoltaic cells by atomic layer deposition. Org Electron 10:1300–1306
109. Luo JX, Xiao LX, Chen ZJ et al (2010) Insulator MnO: highly efficient and air-stable n-type doping layer for organic photovoltaic cells. Org Electron 11:664–669
110. Affinito JD, Gross ME, Coronado CA et al (1996) A new method for fabricating transparent barrier layers. Thin Solid Films 290:63–67
111. Madakasira P, Inoue K, Ulbricht R et al (2005) Multilayer encapsulation of plastic photovoltaic devices. Synth Met 155:332–335